INCORPORATING THE PRE-SYMPTOMATIC STAGE IN THE DISCRETE-TIME KERMACK-MCKENDRICK MODEL

SURIN SINGH

A THESIS SUBMITTED TO
THE FACULTY OF GRADUATE STUDIES
IN PARTIAL FULFILMENT OF THE REQUIREMENTS
FOR THE DEGREE OF
MASTER OF SCIENCE

GRADUATE PROGRAM IN DEPARTMENT OF MATHEMATICS AND STATISTICS
YORK UNIVERSITY
TORONTO, ONTARIO

DECEMBER 2023

Abstract

Numerous mathematical models have been implemented since the COVID-19 pandemic, with most using large compartmental models which indirectly restrict the generation-time distribution. The continuous-time Kermack-McKendrick epidemic model of 1927 (KM27) allows a random generation-time distribution, but there is a disadvantage where the numerical implementation is too much. Here, the pre-symptomatic stage was further included in the recent discrete-time $SEIR$ KM27 Model formulated in Diekmann (2021). With discrete-time models being general, flexible when including public health interventions and easier to implement computationally than continuous-time models, it is a powerful tool for exploring infectious diseases such as COVID-19. To demonstrate this potential, a numerical investigation is performed on how the incidence-peak size depends on the model components. It was found that compartmental models predicted lower peak sizes with the same reproduction number and initial growth rate than models in which the latent, pre-symptomatically infectious and symptomatically infectious periods have fixed duration.

For My Mom and Dad,

I Love You

Acknowledgements

I want to express my heartfelt gratitude to all those who have contributed to the completion of this master's thesis, without whom it would have remained a shelved project. This journey has been challenging and rewarding, and I could not have reached this milestone without the support, guidance, and encouragement of many individuals.

First and foremost, I am deeply indebted to my thesis supervisor, Prof. Jianhong Wu, for his unwavering support and expertise throughout this research. Your guidance, insightful feedback, suggestions, and patience were instrumental in shaping this work. I am fortunate to have had the opportunity to learn from his wealth of knowledge and experience in the field of Infectious Disease Modelling.

I also want to thank the members of my thesis committee, Prof. Huaiping Zhu, Prof. Woldegebriel Assefa Woldegerima and Prof. Marios Fokaefs for your time and effort invested in providing valuable insights and constructive feedback during the evaluation of this thesis. Your expertise enriched the quality of this research and helped me refine my ideas.

I extend my appreciation to the Laboratory for Industrial and Applied Mathematics (LIAM) members for all those Wednesday 2:30 to 3:30 pm meetings and seminars. It provided a conducive academic environment and access to resources that facilitated my research.

I am grateful to all my friends and fellow students who provided moral support, engaging discussion, and occasional moments of respite during this intense academic journey. For a special shoutout to a friend for 12 years now, Mr. Elio Cameron, for constantly asking, 'How is the thesis going?' I know you would enjoy this mention. Your camaraderie made the process more enjoyable and manageable.

Special thanks to my parents, Taij and Nirmala Singh, for their unwavering support, encouragement, and understanding throughout this endeavour. Your belief in my abilities and love motivated me during the most challenging times. I will never forget where I came from. I love you too, Aja, Ajie, Nana and Nanie. I wish you hadn't left so soon and were here to tell me 'Old Guyana stories.'

Lastly, I express my gratitude to all the researchers, scholars, and institutions whose work and publications were instrumental in shaping the background and framework of this thesis.

This thesis represents the collective effort of all those who have guided and supported me along the way. I am deeply appreciative of their contributions.

Thank you all for being a part of this academic journey.

Surin Rohan Singh

Table of Contents

List of Tables

List of Figures

Chapter 1

Introduction

1.1 Discrete-Time Model

Kermack and McKendrick began the study of compartmental epidemic models in the context of single-epidemic outbreaks many decades ago [1]. Fast-forward to the present, infectious diseases such as AIDS, Ebola and COVID-19 are becoming a part of normal life [2]. Tragically, they can spread and result in a great number of deaths. Therefore, it is essential to use the best management methods available to combat these extreme consequences. The only way to try to compare the effectiveness of these methods is to formulate appropriate mathematical models that help us make predictions [3]. Most mathematical models in epidemiology are formulated in continuous time quite possibly because of the amount of analytical tools available for their study [2]. However, the discrete-time model promises to become a powerful tool for exploring control scenarios for specific infectious diseases such as COVID-19 [4].

Continuous-time and discrete-time models are two faces of the same coin. Discrete-time models are represented by systems of difference equations and are more efficient than continuous-time differential equation models because discrete-time models do not require numerically intensive integration [5]. They are easier to implement since the probabilistic background of the models is easily revealed [6]. In comparison, the numerical solutions of continuous-time renewal equations present a great challenge [7].

Although the processes studied take place in continuous time, discrete bookkeeping schemes should be considered in order to relate directly to the data [1, 4]. Census data are often collected

at regular intervals, therefore on a discrete-time basis [4]. These data may be daily or weekly incidence rates in fast-moving epidemics such as influenza, SARS, or Ebola; or monthly or annual rates in slower-moving epidemics such as HIV or Tuberculosis [5]. In long-running epidemics that have a seasonal component, such as Tuberculosis, the effects of seasonality can only be estimated from a model if incidence rates are reported monthly or at least quarterly [8].

The numerical implementation of discrete-time models is straightforward, with simulations being easily performed to compute outbreak dynamics [4]. They are general, flexible and user-friendly when it comes to fitting to epidemic outbreak data rather than continuous-time differential equations. They are also much more readily extended to include heterogeneity such as asymptomatic infection, public health interventions, demographics and other types of stochasticity [4, 9].

Parameters from discrete-time models are related rather directly to surveillance data without the need to make additional model assumptions about the duration of, for instance, the infectious period [4, 10]. Parameters like transmission and recovery rates can be estimated by comparing the discrete model's predictions with observed data and help with understanding the dynamics of the underlying disease. Discrete-time models may not only be widely used to detect the pathogenesis of infectious diseases but also make a great contribution to the prevention and control of infectious diseases [11]. By including different intervention strategies in the model, researchers can simulate their effects and assess their potential effectiveness in diminishing the spread of infectious diseases.

1.2 Motivations and Objectives

As the number of COVID-19 cases increases, physical distancing, washing and sanitizing of hands often, and wearing of face masks are strongly encouraged [12]. The goal of this practice is to flatten the curve of new infections to avoid a surge of demand on the healthcare system, but the effects of physical distancing may take weeks to appear [13]. While many national governments have now put an end to COVID-19 restrictions, scientists have warned that endemic circulation of SARS-CoV-2, perhaps with seasonal epidemic peaks, is likely to have a continued important disease burden [14, 15]. Additionally, virus mutations can be unpredictable, and a lack of effective

surveillance or adequate response could enable the emergence of new epidemics or pandemic COVID-19 patterns [14, 15].

To eliminate the burden on the healthcare system while also providing the best possible care for patients, a reliable prognosis for COVID-19 remains important to inform decisions regarding personal protective equipment (PPE) shortage, vaccination, treatment, and hospital or intensive care unit (ICU) admissions [14, 16].

Healthcare workers rely on PPE such as gloves, medical masks, respirators, goggles, face shields, gowns and aprons to protect themselves and their patients from being infected and infecting others [16-18]. A decline in the supply of healthcare due to worker illness combined with intensified demand for care causes the healthcare infrastructure to become unstable and, therefore, reduces the quality and quantity of care available [17].

To reduce the mounting burden of COVID-19, vaccine development and distribution have occurred at an unprecedented speed and efficiency [19]. Vaccination strategies aim to protect those most vulnerable to severe illness so high-risk groups are those with the utmost importance, such as senior citizens, individuals with underlying health conditions and frontline workers. Strategies may be customized to address specific neighbourhoods, workplaces or educational institution outbreaks. Governments need to have mandatory vaccination policies in place to navigate the waves of the pandemic to help combat the spread of the different variants present [20].

The spread of COVID-19 in China, Italy and the United States of America led to a severe shortage of hospital beds [21-23]. Relative slow government testing has underlined the need to develop region-specific estimates of the number of people that may require hospitalization, plan social-distancing interventions and identify potential shortages of hospital beds [23, 24]. To plan response, hospital and public health officials need to compare how many people in their area are likely to require hospitalization for COVID-19 with how these numbers compare to the number of available intensive care and acute care beds and how to project the impact of social-distancing measures on utilization [23]. With the majority of people with COVID-19 being asymptomatic and the rates of cases requiring hospitalization differing significantly across each age group, answering these questions requires understanding the epidemic [25, 26].

Prediction models that combine several variables or features to estimate the risk of people being infected or experiencing a poor outcome from the infection could assist medical staff in conducting a preliminary assessment of patients when allocating limited healthcare resources [14, 27]. Since the numerical exploration of discrete-time epidemic models is straightforward, it can be easily implemented by non-mathematicians such as those in the public health world [1].

In this thesis, I propose an additional compartment P, pre-symptomatically infectious building upon the discrete-time Kermack-McKendrick $SEIR$ model (KM27) implemented in [4]. I will first show how the peak value of incidence for two types of models and their ratio changes by the different combinations of days latent, pre-symptomatically infectious and symptomatically infectious to prevent overcrowding at hospitals. The two different models being first compared are the 'Block Model', where the length of the latent period and each infectious period is deterministic, and the '$SEPIR$ Model', where these periods are stochastic. Then, I will further investigate the parameters at which the ratio of peak heights is minimal and maximal while showing how the expected contribution to the force of infection is affected by deterministic and stochastic periods. A brief examination of the different prevalence between the two models will be analyzed. Finally, I will perform another comparison with the '$SEPIR$ Model' with stochastic periods to data obtained from [28] while showing one model which was derived from there containing parameters corresponding to the Weibull distribution.

Chapter 2

Background

2.1 Cumulative (over One-Time Step) Force of Infection

From [4], the equation

$$S(t+1) = e^{-\hat{\Lambda}(t)} S(t), \tag{2.1}$$

is used to build the foundation of the discrete-time model for the spread of an infectious disease in a host population when two conditions are met:

- The disease generates permanent immunity
- The host population is demographically closed (meaning that transmission of the disease happens faster than demographic turnover and is therefore ignored)

$S(t)$ is the size of the subpopulation of susceptibles at census time t. Equation (2.1) is the length of the time interval between one census and the next, where $\hat{\Lambda}(t)$ is proportional to the length and is the cumulative force of infection over $(t, t+1]$. Equation (2.1) in continuous time is

$$\frac{dS}{dt}(t) = -\Lambda(t) S(t), \tag{2.2}$$

where $\Lambda(t)$ is the force of infection at time t (probability per unit time for a susceptible to become infected at time t). Solving the differential equation, (2.2) gives

$$S(t+1) = e^{-\int_t^{t+1} \Lambda(\tau)\, d\tau} S(t), \tag{2.3}$$

The probability for a susceptible to escape from infection in the time interval $(t, t+1]$ is given by the first factor at the right-hand side of both equations (2.1) and (2.3).

Further comparison between equations (2.1) and (2.3) gives the following relation

$$\hat{\Lambda}(t) = \int_t^{t+1} \Lambda(\tau)\, d\tau, \tag{2.4}$$

and is the reason why $\hat{\Lambda}(t)$ is called the cumulative force of infection over $(t, t+1]$

Equation (2.2) should not be replaced by the additive differential equation to become

$$S(t+1) - S(t) = -\hat{\Lambda}(t) S(t),$$

which therefore becomes

$$S(t+1) = \left(1 - \hat{\Lambda}(t)\right) S(t), \tag{2.5}$$

but instead, the multiplicative factor present should be adjusted as done in [1].

For very small values of $\hat{\Lambda}(t)$, equation (2.5) provides an excellent approximation to equation (2.1). Otherwise, it may fail greatly and lead to negative values of susceptibles since it does not consider that a host can only be infected once. Whereas equation (2.1) does consider this.

When a single infection is present in a particular host population during a time interval of length one, susceptible hosts become infected with probability p. Therefore, the complementary $1 - p$ is the probability any susceptible does not become infected. If there is contact between I infectious individuals and susceptibles independent of each other, then they don't get infected by probability

$$(1-p)^I = e^{I\, ln(1-p)}$$

A susceptible would therefore be infected with probability $1 - (1-p)^I$ rather than with probability pI.

It should be noted that a lot of heterogeneity is subsumed [4], and individuals may have varying:

1. Degrees of infectiousness

2. Propensity to make contact
3. Their activities may be unevenly distributed over the unit time

As long as I is large and the properties of the two individuals involved in a transmission have independent influence, one can simply interpret p as an average.

From a numerical point of view, the exponential has the disadvantage of being expensive in terms of calculation costs. It may be tempting to reduce the step size to work safely with the linear approximation.

2.2 The General Discrete-Time Kermack-McKendrick Model

The incidence at time t equals $\Lambda(t)S(t)$ with Λ given as the force of infection as seen in equation (2.2). The current force of infection is caused by those who were infected some time ago. Following earlier work by Ross and Hudson [29, 30], Kermack and McKendrick translate this observation which is seen as

$$\Lambda(t) = \int_0^\infty A(\tau)\Lambda(t-\tau)S(t-\tau)\,d\tau, \tag{2.6}$$

where $A(\tau)$ is the expected contribution to the force of infection at time τ after infection. A, the infinite-dimensional parameter is introduced as a key model ingredient. Population-level data can be used to deduce certain characteristics of A [31]. With N representing the population size, the following is obtained

$$R_0 = N\int_0^\infty A(\tau)\,d\tau, \tag{2.7}$$

and in the initial phase of the epidemic, the distribution of the generation-interval has as a density the renormalized function A [32, 33].

Under the assumptions of permanent immunity and no demographic turnover, the incidence equals $-S'$ in equation (2.2). Substituting this into equation (2.6) and integrating, the following identity is obtained

$$\int_t^{t+1} \Lambda(\sigma)\, d\sigma = \int_0^{\infty} A(\tau)[S(t-\tau) - S(t+1-\tau)]\, d\tau, \tag{2.8}$$

The discrete-time version of this is

$$\hat{\Lambda}(t) = \sum_{j=1}^{\infty} A_j [S(t-j) - S(t+1-j)], \tag{2.9}$$

where for an individual, A_j is the expected contribution to the cumulative force of infection over $(t, t+1]$ who became infected in the interval $(t-j, t-j+1]$, j time steps before. $S(t-j) - S(t+1-j)$ is the incidence in $(t-j, t-j+1]$. As mentioned before, the key modelling ingredient is now the collection $\{A_j\}_{j=1}^{\infty}$ of nonnegative numbers, where it is assumed that

$$\sum_{j=1}^{\infty} A_j < \infty,$$

A_k may depend on calendar time due to control measures or seasonality [4].

Stating an initial condition for the history of S up to a certain point in time provides an updating scheme. The prescribed history should be a monotone nondecreasing (when looking back into time) sequence, bounded from above by the total host population size *N* and taking equation (2.1) with $\hat{\Lambda}(t)$ specified by equation (2.9), the following scalar higher-order recursion relation is obtained

$$s(t+1) = e^{-\sum_{k=1}^{\infty}(1-s(t-k+1))\tilde{A}_k}, \tag{2.10}$$

where,

$$s(t) = \frac{S(t)}{N}, \tag{2.11}$$

and

$$\tilde{A}_k = A_k N, \tag{2.12}$$

Equation (2.10) is the discrete-time version of the nonlinear renewal equation,

$$s(t) = e^{-\int_0^{\infty}(1-s(t-\tau))NA(\tau)\, d\tau}, \tag{2.13}$$

by combining equation (2.2) with (2.9) and incidence equal to $-S'$ [7, 34]. There is an extra assumption

$$S(-\infty) = N, \tag{2.14}$$

that says all hosts were susceptible in the infinite past. This is used in both equations (2.10) and (2.13). In the process of deriving equation (2.10) while equation (2.14) holds, first note that iteration of (2.1) gives the identity

$$s(t+1) = e^{-\sum_{i=0}^{\infty} \hat{\Lambda}(t-i)} N. \tag{2.15}$$

Using equation (2.9), the following is derived

$$\begin{aligned}\sum_{i=0}^{\infty} \hat{\Lambda}(t-i) &= \sum_{i=0}^{\infty}\sum_{k=1}^{\infty} A_k[S(t-i-k) - S(t-i-k+1)] \\ &= \sum_{k=1}^{\infty} A_k \sum_{k=1}^{\infty}[S(t-i-k) - S(t-i-k+1)] \\ &= \sum_{k=1}^{\infty} A_k[S(t-i-k) - S(t-i-k+1)]\end{aligned}$$

By dividing by N on both sides of equation (2.15) and using the notation of equation (2.11) and equation (2.12), equation (2.10) can be derived. By replacing $t+1$ in equation (2.10) with t and merging the two formulas, a variant can be derived,

$$s(t+1) = s(t)e^{-\sum_{k=1}^{\infty}(s(t-k)-s(t-k+1))\tilde{A}_k}. \tag{2.16}$$

This equation has the advantage where one can provide an initial condition, say at time 0, by specifying $s(0)$ and the (nonnegative) incidences $\ldots, s(-3) - s(-2)$, $s(-2) - s(-1)$, $s(-1) - s(0)$. Equations (2.10) and (2.16) are the mathematical form of the discrete-time KM27 model with $\{A_k\}_{k=1}^{\infty}$, a countable infinite parameter in principle, but in practice, a finite, m, dimensional parameter with an infinite tail of zeros.

The homogeneous version is the simplest form, but heterogeneity can be added and further explained in the discrete-time bookkeeping scheme.

2.3 The Initial Phase and the Final Size

During the early stages of an infectious disease being introduced to a host population, the branching process is necessary to capture the demographic stochasticity [34]. A more deterministic approach must be used when there are many infected individuals in the population. This large number still accounts for a rather small fraction of a substantial host population. By putting

$$s(t) = 1 - x(t), \tag{2.17}$$

into equation (2.10), and an assumption is made that x is so small that the exponential is replaced by the zeroth and first-order terms of the Taylor expansion. This results in the linearized equation,

$$x(t+1) = \sum_{k=1}^{\infty} \tilde{A}_k x(t-k+1), \tag{2.18}$$

R_0 is defined as the average number of new infections generated by a single infected individual introduced into an entirely susceptible population [35], and is given as

$$R_0 = \sum_{k=1}^{\infty} \tilde{A}_k = \sum_{k=1}^{\infty} A_k N, \tag{2.19}$$

An assumption

$$x(t) = \lambda^t, \tag{2.20}$$

is made to show that positive solutions decline when $R_0 < 1$ and grow when $R_0 > 1$ in equation (2.18). The x defined in equation (2.20) is indeed a solution if and only if λ is a real root of the discrete-time characteristic equation (Euler-Lotka equation)

$$1 = \sum_{k=1}^{\infty} \lambda^{-k} \tilde{A}_k, \tag{2.21}$$

when equation (2.20) is substituted into equation (2.18). Because $\tilde{A}_k, k = 1,2, \ldots$, is nonnegative, it means that (2.21) has at most one real root ρ. For the case where $R_0 > 1$, it does have a real root when the right-hand side has a bigger value than one for some real λ. For the cases when $\tilde{A}_k$ has power-like behaviour for $k \to \infty$ and $R_0 < 1$, the value of the right-hand side may go from a value

less than one to infinity when λ decreases but when $\tilde{A}_k = 0$ for large k, this doesn't happen and ρ exists. For a real λ, the right-hand side of equation (2.21) is a monotone decreasing function and can be summarized as

$$sign(\rho - 1) = sign(R_0 - 1) \tag{2.22}$$

In continuous-time theory, ρ relates to e^r, where r is the Malthusian parameter. General linear theory assures that solutions which are positive for equation (2.18) grow geometrically with rate ρ for $t \to \infty$ when $\rho > 1$ and would decrease with rate ρ, when ρ exists and $\rho < 1$ [36]. General nonlinear theory assures that the steady-state solution $s(t) \equiv 1$ of equation (2.10) is asymptotically stable for $\rho < 1$, therefore $R_0 < 1$, but unstable for $\rho > 1$, therefore $R_0 > 1$ [37]. For the version with only finitely many A_k different from zero, the standard Hartman-Grobman Theorem implies that the intersection of the positive cone and the unstable manifold is one-dimensional, meaning that there is one positive solution of equation (2.10) that has a limit of 1 for $t \to -\infty$ [4].

With the introduction of the pathogen and when $R_0 > 1$, it can cause s to decrease to below 1. This reinforces the idea that s is a monotone decreasing function of time and its limit $t \to \infty$, is written as $s(\infty)$.

$$s(\infty) = e^{-R_0(1-s(\infty))}, \tag{2.23}$$

This equation is acquired by passing to the limit in equation (2.10) and by using the idea that $\{\tilde{A}_k\}$ is summable. This equation has a unique solution in $(0, 1)$ when $R_0 > 1$ [34].

When the continuous-time and discrete-time formulations are compared,

- There is only a formal difference in the expressions for R_0
- If $\rho = e^r$, there is only a formal difference in the equations characterizing, respectively ρ and r
- The equations specifying $s(\infty)$ on the basis of R_0 are identical [1]

So, at the level of theory, there is an exact parallel for the two formulations [4].

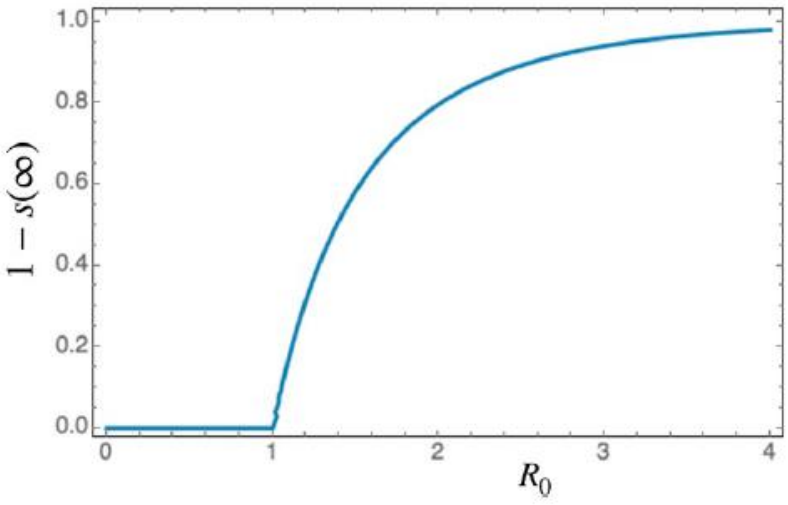

Figure 2.1: Graph of the final size $1 - s(\infty)$, (the fraction of the population that gets infected in the course of the outbreak, as a function of the basic reproduction number R_0 [4].

2.4 Compartmental Formulation for Some Very Special Cases

The general pattern of constructing discrete-time models in a compartmental setting is explained using a SIR and $SEIR$ model

2.4.1 SIR Model

When an individual gets infected, they are transferred from compartment S to I, which contains the infected individuals. Individuals may lose infectiousness either by recovery or death with probability α or stay infected with probability $1-\alpha$. Removed individuals are placed in compartment R, where immunity is permanent. The per capita contribution to the force of infection equals β while the cumulative force of infection equals βI. β is proportional to the time between census points (length of the discretization interval) and $\alpha = 1 - e^{-\tilde{\alpha}}$ with $\tilde{\alpha}$ proportional to its length.

Due to these assumptions, the system of recurrence relations is:-

$$S(t+1) = e^{-\beta I(t)} S(t),$$

$$I(t+1) = \left(1 - e^{-\beta I(t)}\right)S(t) + (1-\alpha)I(t)$$

$$R(t+1) = \alpha I(t) + R(t) \tag{2.23}$$

By choosing an appropriate $\tilde{A}_k$ equation (2.24), the system (2.23) may be reduced to the scalar recurrence equation, (2.10).

$$\tilde{A}_k = \beta(1-\alpha)^{k-1}N \tag{2.24}$$

Iterating $S(t+1)$ in the system (2.23) with the derivation of equation (2.15),

$$S(t+1) = e^{-\beta \sum_{j=0}^{\infty} I(t-j)}N$$

is obtained.

$$I(t+1) = S(t) - S(t+1) + (1-\alpha)I(t),$$

is the rewritten form for the second equation in the system (2.23). This is obtained by summing the identity

$$\sum_{j=0}^{\infty} I(t-j) = N - S(t) + (1-\alpha)\sum_{j=0}^{\infty} I(t-j-1)$$

Using equation (2.10) with $\tilde{A}_k$ given by equation (2.24), equation (2.23) is easily recovered by

$$I(t) = \sum_{k=1}^{\infty}[S(t-k) - S(t-k+1)](1-\alpha)^{k-1} \tag{2.25}$$

$R(t)$ is the rate of individuals that are no longer infectious and does not affect $S(t)$ and $I(t)$.

If $e^{-\beta I(t)}$ is replaced by $1 - \beta(t)$, the reduction to a higher-order scalar recursion relation fails [4].

2.4.2 *SEIR* Model with Stochastic Periods

To take into consideration the latent period, the $SEIR$ model is used. When an individual is infected but not yet infectious, they enter compartment E of exposed individuals. The system of recurrence relations (2.23) is adjusted when the length of the latent period is geometrically distributed with γ to give:

$$S(t+1) = e^{-\beta I(t)} S(t),$$

$$E(t+1) = \left(1 - e^{-\beta I(t)}\right) S(t) + (1-\gamma) E(t)$$

$$I(t+1) = \gamma E(t) + (1-\alpha) I(t)$$

$$R(t+1) = \alpha I(t) + R(t), \tag{2.26}$$

Individuals can be in states S, E, I, and R when thinking in terms of a stochastic process. It is helpful enough just thinking about E and I since there is interest when an individual becomes infected, and this stops when they lose infectiousness. If E is labelled as index 1 and I is index 2, then the probability distribution of the state-at-infection is represented by the vector,

$$\begin{bmatrix} 1 \\ 0 \end{bmatrix}.$$

The following matrix describes the state transitions

$$M = \begin{bmatrix} 1-\gamma & 0 \\ \gamma & 1-\alpha \end{bmatrix},$$

and infectiousness by vector

$$b = [0 \quad \beta].$$

After becoming infected, the expected infectiousness k units of time are

$$A_k = bM^{k-1} \begin{bmatrix} 1 \\ 0 \end{bmatrix}$$

$$A_k = \beta \sum_{l=1}^{k-1} \gamma (1-\gamma)^{l-1} (1-\alpha)^{k-1-l}, \tag{2.27}$$

When $\tilde{A}_k$ has the form defined by equations (2.12) and (2.27), then the system (2.26) follows from equation (2.10) if the following is defined as

$$E(t) = \sum_{j=1}^{\infty} [S(t-j) - S(t-j+1)](1-\gamma)^{j-1},$$

$$I(t) = \sum_{j=1}^{\infty} \left([S(t-j) - S(t-j+1)] . \sum_{l=1}^{\infty} \gamma (1-\gamma)^{l-1} (1-\alpha)^{j-1-l} \right). \tag{2.28}$$

Using the explicit expression of the A_k for the $SEIR$ model, equation (2.27), the relationship can be determined between α, β and γ on one hand, and ρ on the other, using the Euler-Lotka equation (2.21),

$$\frac{1}{N} = \frac{\beta\gamma}{(\rho+\alpha-1)(\rho+\gamma-1)}$$

From equation (2.19) for R_0, the familiar expression $R_0 = \frac{\beta N}{\alpha}$ is obtained and substituting this into the above expression gives

$$\alpha = \frac{(\rho+\gamma-1)(\rho-1)}{1-\rho+\gamma(R_0-1)}$$

$$\beta = \frac{R_0}{N}\frac{(\rho+\gamma-1)(\rho-1)}{1-\rho+\gamma(R_0-1)}$$

Lastly, the link between γ and T_E is simply:

$$\gamma = \frac{1}{T_E}$$

So, in all, T_E, ρ, and R_0 define the parameters for the $SEIR$ model.

Where,

T_E = Number of days an individual is exposed but not yet infectious,

$\tilde{A}_k$ is therefore given by

$$\tilde{A}_k = \frac{R_0}{T_E}\frac{(\rho+\gamma-1)(\rho-1)}{\left(1-\rho+\gamma(R_0-1)\right)}\sum_{l=1}^{k-1}\left(1-\frac{1}{T_E}\right)^{l-1}\left(1-\frac{(\rho+\gamma-1)(\rho-1)}{1-\rho+\gamma(R_0-1)}\right)^{k-l-1} \quad (2.29)$$

2.4.3 $SEIR$ Model with Deterministic Periods

Another model is also defined by prescribing the values of the rescaled expected contribution to the force of infection, $\tilde{A}_k$, where k is the number of days that have elapsed since becoming infected. With T_E as defined previously and T_I being the number of days an individual is infectious, in this

model, these two periods are assumed to be the same for all individuals (deterministic) and the following is set:

$$\begin{aligned} \tilde{A}_k &= 0, && 1 \le k \le T_E, \\ \tilde{A}_k &= \tfrac{R_0}{T_I}, && T_E + 1 \le k \le T_E + T_I, \\ \tilde{A}_k &= 0, && k \ge T_E + T_I + 1, \end{aligned} \tag{2.30}$$

2.5 On the Choice of Parameters A_k

The components $\{A_k\}$ include mechanistic properties of the process of contact between hosts, as well as physiological/immunological properties within-hosts dynamics [4]. Unfortunately, information about such properties is limited, and educated guesses need to be made [38].

The SIR and $SEIR$ models explained before have the advantage of just containing a few parameters but can be wrongly educated guesses [4]. A_k represents averages, and if on day four after infection, only 15% of the infected individuals are infectious, while on day five, it rises to 30%, this information is useful for the choice of A_k. If it is known that the degree of infectiousness differs between individuals on days four and five, the guesstimated average can still be used.

To give a more theoretical example, suppose that a fraction p of the infected individuals is asymptomatic and a symptomatic individual has at day j after infection a probability θ_j to be detected and put into quarantine. Assume $\{B_k\}$ is given as the intrinsic infectiousness and contact intensity of symptomatic and asymptomatic cases and are identical, then A_k is given as

$$A_k = \left(p + (1-p) \prod_{j=1}^{k} \left(1 - \theta_j\right) \right) B_k \tag{2.31}$$

Equation (2.31) is based on the questionable assumption that at the day of its detection, an individual doesn't contribute to the force of infection. This weakness can be rectified but at the price of introducing yet another parameter.

The parameters θ_j can capture the effect of testing. During a pandemic such as COVID-19, the testing capabilities depend on calendar day [4, 39]. This results in parameters θ_j having time

dependency. Control measures that reduce contact opportunities affect the B_k in a time-dependent multiplicative manner.

2.6 Reformulation as a First-Order System

A first-order system of equations is more suitable for computation, while the higher-order recursion relation, equation (2.10) is more suited for theoretical purposes. A finite-dimensional system is suitable, and an assumption that the indices j for when A_j is strictly positive have a finite upper bound. Where an integer m exists such that $A_j = 0$ for all $j \geq m + 1$. As a result, the history of S, which matters for determining the future, has a finite length.

$$X_j(t) \coloneqq s(t + 1 - j), \quad j = 1, \dots, m \tag{2.32}$$

Much of the dynamics of vector X amounts to shifting:

$$X_j(t + 1) = X_{j-1}(t), \quad j = 2, \dots, m \tag{2.33}$$

Combining equations (2.1), (2.11), (2.12) and (2.16) gives the rule for extension

$$X_1(t + 1) = X_1(t) e^{-\sum_{j=1}^{m} \tilde{A}_j \left(X_{j+1}(t) - X_j(t)\right)} \tag{2.34}$$

It is harmless to allow $\tilde{A}_j$ to depend on time t in equation (2.34)

On the other hand, by starting from equation (2.16) and choosing

$$X_1(t) = s(t) \tag{2.35}$$

But for $j > 1$

$$X_j(t) = s(t + 1 - j) - s(t + 2 - j), \tag{2.36}$$

which relates to the incidence in time interval $(t + 1 - j,\ t - j + 2]$. The cumulative force of infection with the choice of $X_j(t)$ becomes

$$\hat{\Lambda}(t) = \sum_{j=1}^{m} A_j X_{j+1}(t). \tag{2.37}$$

Which leads to the rules being updated

$$X_1(t+1) = X_1(t)e^{-\sum_{k=1}^{m} \tilde{A}_k X_{k+1}(t)} \tag{2.38}$$

$$X_2(t+1) = X_1(t) - X_1(t+1), \tag{2.39}$$

$$X_j(t+1) = X_{j-1}(t), \;\; j > 2 \tag{2.40}$$

$\tilde{A}_k$ can be allowed to depend on time t in this formulation [4].

2.7 Weibull Distribution

The Weibull distribution used here is a two-parameter family of curves and is a continuous probability distribution that can fit an extensive range of distribution shapes [40, 41]. Like the normal distribution, the Weibull distribution is unimodal and describes probabilities associated with continuous data. However, unlike the normal distribution, it can also model skewed data [41]. Because of the flexibility of the Weibull distribution, it is commonly used in fracture mechanics, actuarial studies and many other fields. [42-44].

The probability density function of the Weibull distribution is given by

$$g(\tau) = \begin{cases} \frac{b}{a}\left(\frac{\tau}{a}\right)^{b-1} e^{-\left(\frac{\tau}{a}\right)^{b}} & if \;\; \tau \geq 0 \\ 0 & if \;\; \tau < 0 \end{cases} \tag{2.41}$$

where a is known as the scale parameter and b controls the shape of the distribution and is called the shape parameter.

In [28], the generation interval distribution $g(\tau)$ is approximated by a Weibull distribution. It is discretized by,

$$g_k = \int_{k-1}^{k} g(\tau)\, d\tau\,, \qquad k \;=\; 1,2,\ldots \tag{2.42}$$

The expected contribution to the force of infection is then given as,

$$\tilde{A}_k = R_0 g_k, \;\; k \;=\; 1,2,\ldots \tag{2.43}$$

Chapter 3

Methods

3.1 Model Description: $SEPIR$ Model with Stochastic Periods

By incorporating the pre-symptomatic infectiousness (P) state, representing the infectiousness before symptom onset of SARS-CoV-2 into the classic $SEIR$ model, the $SEPIR$ (Susceptible, Exposed, Pre-symptomatically Infectious, Symptomatically Infectious, Recovered) model is developed [45].

3.1.1 Model Assumptions

Similar to [4], the following key assumptions were made in constructing the model:

- The disease generates permanent immunity
- The host population is demographically closed

Variable	Description
S	Individuals who are susceptible to infection and have not yet been infected
E	Individuals who are infected, but not yet infectious
P	Individuals who are infected and infectious, but have not yet developed symptoms
I	Individuals who are infected and infectious and have developed symptoms
R	Individuals who have been removed therefore lose infectiousness either by way of the immune system conquering the pathogen or by death

Table 3.1: Description of the basic model state variables.

Figure 3.1: A basic schematic diagram of the $SEPIR$ model dynamics.

The system of recurrence relations (2.26) in the $SEIR$ model is replaced by the new recurrence relations (3.1) for the $SEPIR$ model.

$$S(t+1) = S(t)e^{-(\beta_P P(t)+\beta_I I(t))},$$

$$E(t+1) = S(t)\left(1 - e^{-(\beta_P P(t)+\beta_I I(t))}\right) + (1-\gamma)E(t),$$

$$P(t+1) = \gamma E(t) + (1-\delta)P(t),$$

$$I(t+1) = \delta P(t) + (1-\alpha)I(t),$$

$$R(t+1) = \alpha I(t) + R(t), \tag{3.1}$$

Two terms are going from S to E: consisting of those infected by someone in P with transmission rate β_P, and those infected by someone in I with transmission rate β_I. γ is the probability of becoming pre-symptomatically infectious, δ is the probability of becoming symptomatically infectious and α is the probability of being removed.

It is helpful enough to think about just states E, P and I when developing the model, since there is interest when an individual becomes infected, and this is lost when they lose infectiousness. If E is labelled as index 1, P as index 2 and I is index 3, then the probability distribution of the state-at-infection is represented by,

$$\begin{bmatrix}1\\0\\0\end{bmatrix}$$

The state transitions are described by,

$$M = \begin{bmatrix}1-\gamma & 0 & 0\\ \gamma & 1-\delta & 0\\ 0 & \delta & 1-\alpha\end{bmatrix}$$

and infectiousness by the vector,

$$b = \begin{bmatrix}0 & \beta_p & \beta_I\end{bmatrix},$$

After becoming infected, the expected infectiousness k units of time is:

$$A_k = bM^{k-1}\begin{bmatrix}1\\0\\0\end{bmatrix},$$

$$A_k = \gamma \sum_{l=1}^{k-1} \Big(\beta_P (1-\delta)^{l-1}(1-\gamma)^{k-1-l} + \frac{\beta_I \delta}{\alpha-\delta}\left[(1-\delta)^{l-1}(1-\gamma)^{k-1-l} - (1-\gamma)^{l-1}(1-\alpha)^{k-1-l}\right]\Big), \tag{3.2}$$

When $\tilde{A}_k$ has the form defined by equations (2.12) and (3.2), then the system (3.1) follows from (2.10) if the following is defined as

$$E(t) = \sum_{j=1}^{\infty}[S(t-j) - S(t-j+1)](1-\gamma)^{j-1},$$

$$P(t) = \sum_{j=1}^{\infty}\left([S(t-j) - S(t-j+1)].\sum_{l=1}^{\infty}\gamma(1-\delta)^{l-1}(1-\gamma)^{j-1-l}\right),$$

$$I(t) = \sum_{j=1}^{\infty}\left([S(t-j) - S(t-j+1)].\sum_{l=1}^{\infty}\left(\frac{\gamma\delta}{\alpha-\delta}\right)\left[(1-\delta)^{l-1}(1-\gamma)^{j-1-l} - (1-\gamma)^{l-1}(1-\alpha)^{j-1-l}\right]\right) \tag{3.3}$$

Using the explicit expression of the A_k for the $SEPIR$ model, equation (3.2), the relationship between $\alpha, \beta_P, \beta_I, \delta$ and γ can be determined on one hand, and ρ on the other using the Euler-Lotka equation (2.21),

$$\frac{1}{N} = \frac{\beta_p \gamma}{(\rho + \gamma - 1)(\rho + \delta - 1)} + \frac{\beta_I \gamma \delta}{(p + \gamma - 1)(\rho + \delta - 1)(\rho + \alpha - 1)}$$

From equation (2.19) for R_0, the expression

$$R_0 = N\left(\frac{\beta_P}{\delta} + \frac{\beta_I}{\alpha}\right)$$

is obtained and substituting this into the above expression gives

$$\beta_P = \frac{(\rho + \gamma - 1)(\rho + \delta - 1)(\rho + \alpha - 1) - \gamma\delta\alpha R_0}{N\gamma(\rho - 1)}$$

$$\beta_I = \frac{\alpha(\rho + \alpha - 1)[\gamma\delta R_0 - (\rho + \gamma - 1)(\rho + \delta - 1)]}{N\gamma\delta(\rho - 1)}$$

The link between γ and T_E, δ and T_P and α and T_I is simply:

$$\gamma = \frac{1}{T_E}$$

$$\delta = \frac{1}{T_P}$$

$$\alpha = \frac{1}{T_I}$$

T_E = Number of days an individual is exposed, but not yet infectious

T_P = Number of days an individual is pre-symptomatically infectious

T_I = Number of days an individual is symptomatically infectious

The latent period is T_E and the incubation period is $T_E + T_P$.

$\tilde{A}_k$ is given by,

$$\tilde{A}_k = \frac{1}{\rho - 1} \sum_{l=1}^{k-1} \Bigg(\big((\rho+\gamma-1)(\rho+\delta-1)(\rho+\alpha-1) - \gamma\delta\alpha R_0\big) \left(1 - \frac{1}{T_p}\right)^{l-1} \left(1 - \frac{1}{T_E}\right)^{k-1-l}$$

$$+ \frac{\alpha(\rho+\alpha-1)[\gamma\delta R_0 - (\rho+\gamma-1)(\rho+\delta-1)]}{\alpha-\delta} \Bigg[\left(1 - \frac{1}{T_P}\right)^{l-1} \left(1 - \frac{1}{T_E}\right)^{k-1-l}$$

$$- \left(1 - \frac{1}{T_E}\right)^{l-1} \left(1 - \frac{1}{T_I}\right)^{k-1-l} \Bigg] \Bigg) \tag{3.4}$$

3.2 $SEPIR$ Model with Deterministic Periods ('Block Model')

Later, two types of models will be numerically compared where they have the same initial rate of increase ρ and basic reproduction number R_0 but different expected contributions to the force of infection, $\tilde{A}_k$. These two models are defined by prescribing the values of the rescaled expected contribution to the force of infection, $\tilde{A}_k$, where k is the number of days that have elapsed since becoming infected. With T_E, T_P and T_I just defined, in this model these three periods are assumed to be the same for all individuals (deterministic) and the following is set

$$\begin{aligned}
&\tilde{A}_k = 0, && 1 \le k \le T_E, \\
&\tilde{A}_k = \tfrac{R_0}{2T_P}, && T_E + 1 \le k \le T_E + T_P, \\
&\tilde{A}_k = \tfrac{R_0}{2T_I}, && T_E + T_P + 1 \le k \le T_E + T_P + T_I, \\
&\tilde{A}_k = 0, && k \ge T_E + T_P + T_I + 1,
\end{aligned} \tag{3.5}$$

From here onwards, the 'Block Model' refers to the $SEPIR$ model with deterministic periods.

3.3 Model Parameters

Parameter	Description		Value	Reference
R_0	Reproduction number		2.5	[4]
ρ	Initial growth rate:	with T_I = 8 with T_I = 9 with T_I = 10	1.0724 – 1.1639 1.0714 – 1.1600 1.0705 – 1.1564	Computed based on initial conditions
β_P	Pre-symptomatic transmission rate:	with T_I = 8 with T_I = 9 with T_I = 10	0.2253 – 0.5284 0.2266 – 0.5248 0.2274 – 0.5212	Computed based on initial conditions
β_I	Symptomatic transmission rate:	with T_I = 8 with T_I = 9 with T_I = 10	0.0924 – 0.1489 0.0832 – 0.1300 0.0758 – 0.1155	Computed based on initial conditions
$1/\gamma$	Mean latent period		2 – 6 days	Assumed
$1/\delta$	Mean infectious period of pre-symptomatic infection		3 – 7 days	Assumed
$1/\alpha$	Mean infectious period of symptomatic infection		8 – 10 days	Assumed

Table 3.2: Description of the model parameters and their values when comparing the 'Block Model' with deterministic periods and the '$SEPIR$ Model' with stochastic periods.

Parameter	Description	Value	Reference
R_0	Reproduction number	2.5	[4]
ρ	Initial growth rate	1.1961	[28]
β_P	Pre-symptomatic transmission rate	0.6184 – 1.1327	Computed based on initial conditions
β_I	Symptomatic transmission rate	0.0033 – 0.1709	Computed based on initial conditions
$1/\gamma$	Mean latent period	2 days	Assumed
$1/\delta$	Mean infectious period of pre-symptomatic infection	1 – 4 days	Assumed
$1/\alpha$	Mean infectious period of symptomatic infection	8 days	Assumed

Table 3.3: Description of the model parameters and their values when comparing the '$SEPIR$ Model' with stochastic periods to the 'Actual Data' obtained from [28].

Parameter	Description	Value	Reference
a	Weibull scale parameter	5.665	[28]
b	Weibull shape parameter	2.826	[28]
ρ	Initial growth rate	1.1919	[28]
β_P	Pre-symptomatic transmission rate	0.6028 – 1.0954	Computed based on initial conditions
β_I	Symptomatic transmission rate	0.0111 – 0.1756	Computed based on initial conditions

Table 3.4: Description of the model parameters and their values for the 'Weibull' Model corresponding to the Weibull distribution obtained from [28] (The reproduction number, mean latent and different infectious periods are the same as in Table 3.3).

Chapter 4

Results

4.1 About the Peak of the Incidence Curve

Many features are present on an epidemic curve, such as:

1. The initial growth rate ρ

2. The height and timing of the peak

3. The final size

It is easily recognized that the initial growth rate and final size are related to simple models' parameters that don't consider heterogeneity. For example, R_0 entirely determines the final size while a solution of the Euler-Lotka equation is ρ.

At the beginning of an outbreak an initial growth rate is observed and using information about the generation interval conclusions about R_0 can be made. Model parameters such as R_0 and ρ can be chosen to relate to the estimated values. Due to the COVID-19 pandemic, there is a significant concern in peaks because there may be a PPE shortage, vaccination strategies may be ignored, and hospitals may be overcrowded with patients resulting in the healthcare system collapsing. Determining the timing and height of peaks from a model's parameter is a difficult task using analytical methods [4]. Instead, numerical calculations are used.

The major question answered in this section is: How much is peak height influenced by model details? A comparison is made between the discrete-time compartmental model corresponding to geometric distributions of the latent, pre-symptomatically infectious and symptomatically infectious period lengths alongside a model where these periods are fixed, and the infectiousness is constant during each infectious period.

4.2 Initial Conditions for Simulations

All simulations were conducted in a total population ratio of 1 and with $R_0 = 2.5$. For the initial condition, a short history of decreasing fractions of susceptibles reflects an exponential increase in new cases at the rate ρ. Equation (2.16) was used to carry out the numerical simulations using an initial condition in which the epidemic has started increasing at a rate ρ for six days:

$$s(t) = 1 - 0.00001\rho^{t+6}, \qquad t = -1, -2, \dots, -6 \tag{4.1}$$

All simulations ran for 200 days. The simulation also ran with different initial conditions (See Appendix A). These initial conditions described here were implemented in MATLAB© to simulate the models and to obtain the results.

4.3 Results

4.3.1 'Block Model' with Deterministic Periods and '$SEPIR$ Model' with Stochastic Periods

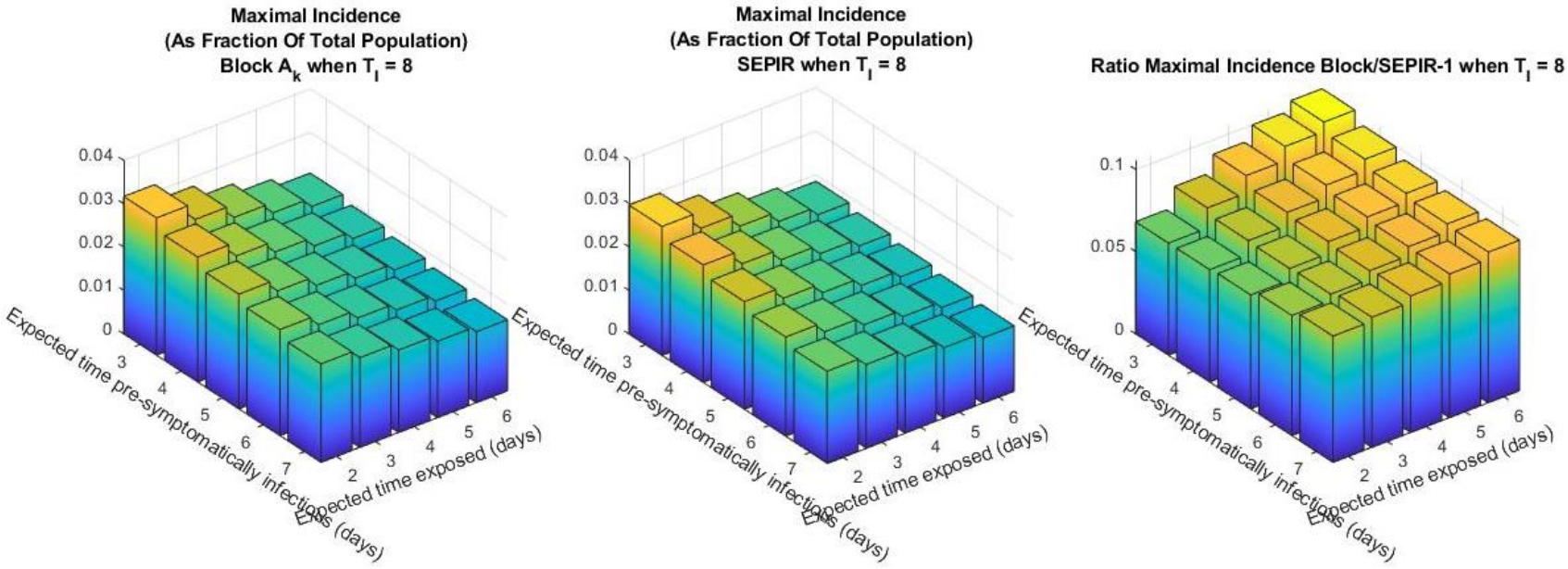

Figure 4.1: Comparing incidences between two types of models when $T_I = 8$. In the 'Block Model', the lengths of the latent, pre-symptomatically infectious and symptomatically infectious periods are deterministic (fixed for all individuals). In the '$SEPIR$ Model', the lengths of these periods are stochastic (independently exponentially distributed with identical parameters, respectively, $1/T_E$, $1/T_P$ and $1/T_I$. **Left:** Here is the maximum incidence of the 'Block Model' with deterministic periods. **Middle:** The maximum incidence of the '$SEPIR$ Model' with stochastic periods. **Right:** The relative ratio between the two, $\frac{block-SEPIR}{SEPIR}$, as a function of T_E, the expected time individuals are exposed and T_P, the expected time individuals are pre-symptomatically infectious. Models were compared after ensuring that they have the same R_0 and initial growth rate ρ.

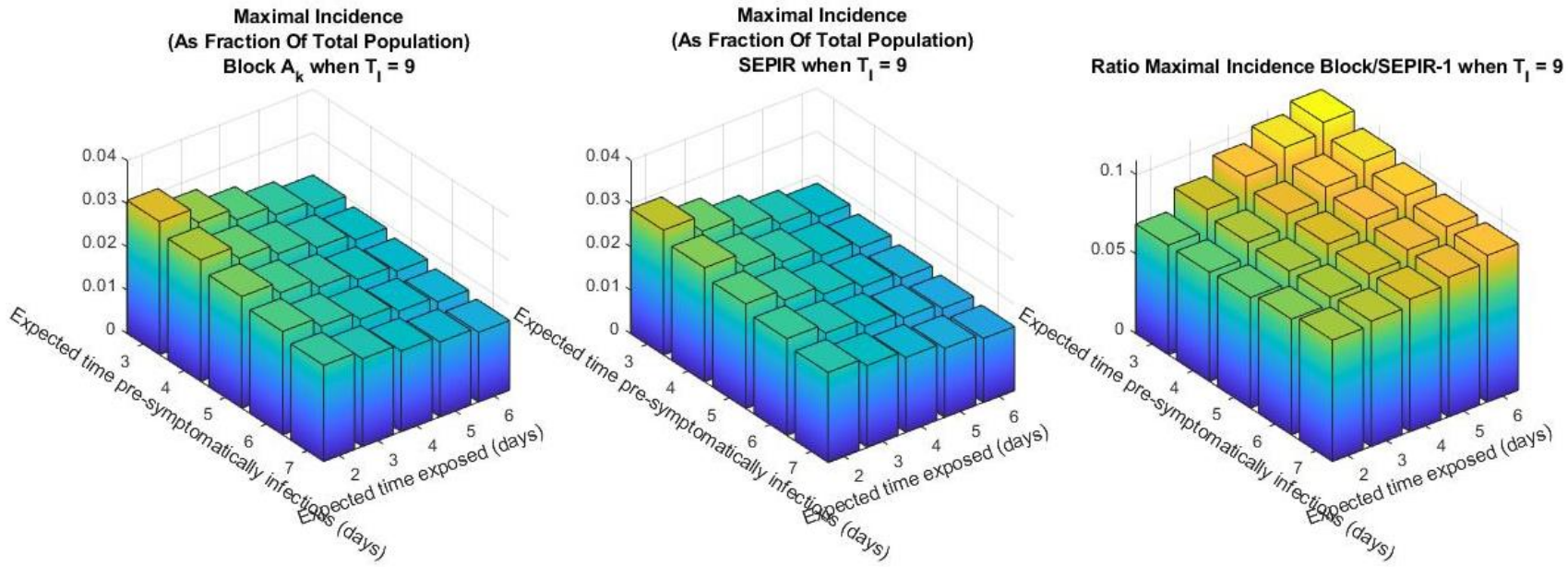

Figure 4.2: Comparing incidences between two types of models when $T_I = 9$.

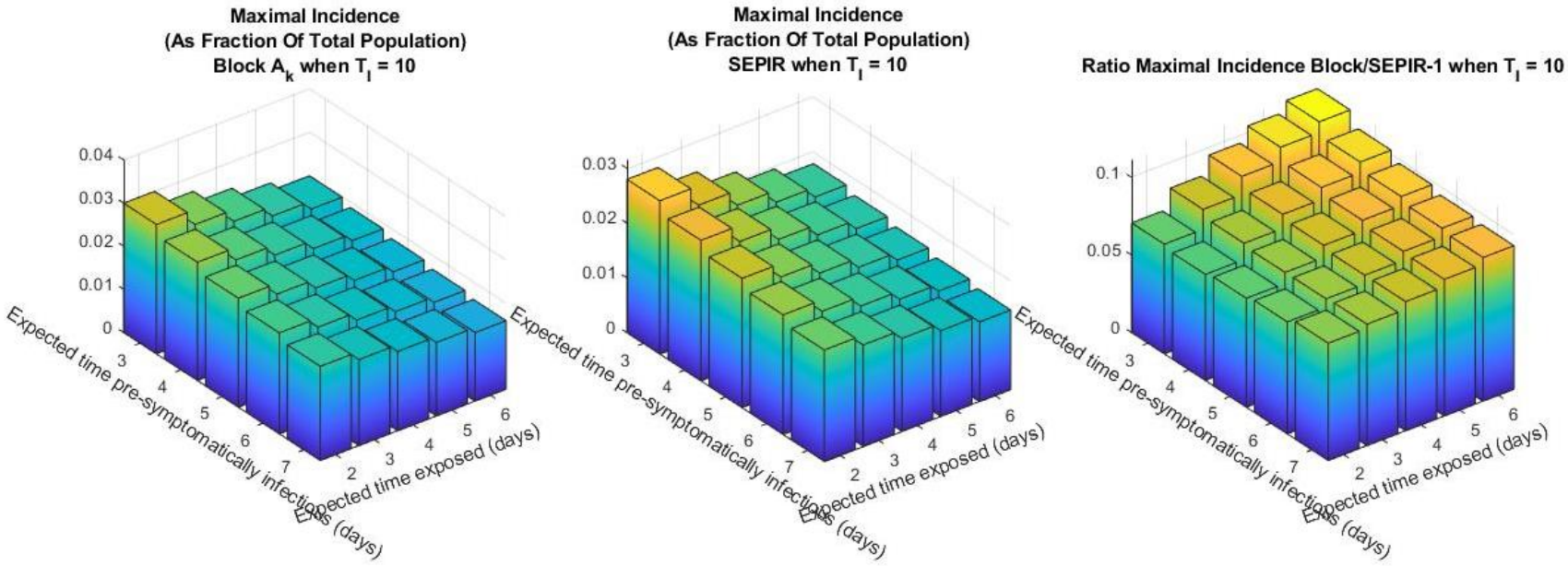

Figure 4.3: Comparing incidences between two types of models when $T_I = 10$.

$T_E \backslash T_P$	3	4	5	6	7
2	0.0681	0.0683	0.0692	0.0730	0.0768
3	0.0805	0.0769	0.0763	0.0769	0.0792
4	0.0911	0.0850	0.0835	0.0821	0.0832
5	0.0997	0.0925	0.0895	0.0877	0.0874
6	0.1055	0.0992	0.0948	0.0924	0.0916

Table 4.1: The relative ratio of the peak height of the two models ('Block Model' with deterministic periods and the '$SEPIR$ Model' with stochastic periods) corresponding to Figure 4.1 when the expected time individuals are symptomatically infectious, $T_I = 8$ as a function of T_E, the expected time individuals are exposed and T_P, the expected time individuals are pre-symptomatically infectious.

$T_E \backslash T_P$	3	4	5	6	7
2	0.0688	0.0686	0.0695	0.0726	0.0762
3	0.0821	0.0780	0.0768	0.0772	0.0788
4	0.0933	0.0866	0.0844	0.0826	0.0833
5	0.1022	0.0942	0.0907	0.0882	0.0877
6	0.1086	0.1010	0.0962	0.0933	0.0921

Table 4.2: The relative ratio of the peak height of the two models when $T_I = 9$ corresponding to Figure 4.2.

$T_E \backslash T_P$	3	4	5	6	7
2	0.0707	0.0684	0.0702	0.0722	0.0756
3	0.0835	0.0789	0.0773	0.0775	0.0783
4	0.0953	0.0880	0.0852	0.0831	0.0833
5	0.1045	0.0958	0.0918	0.0889	0.0881
6	0.1113	0.1026	0.0975	0.0943	0.0926

Table 4.3: The relative ratio of the peak height of the two models when $T_I = 10$ corresponding to Figure 4.3.

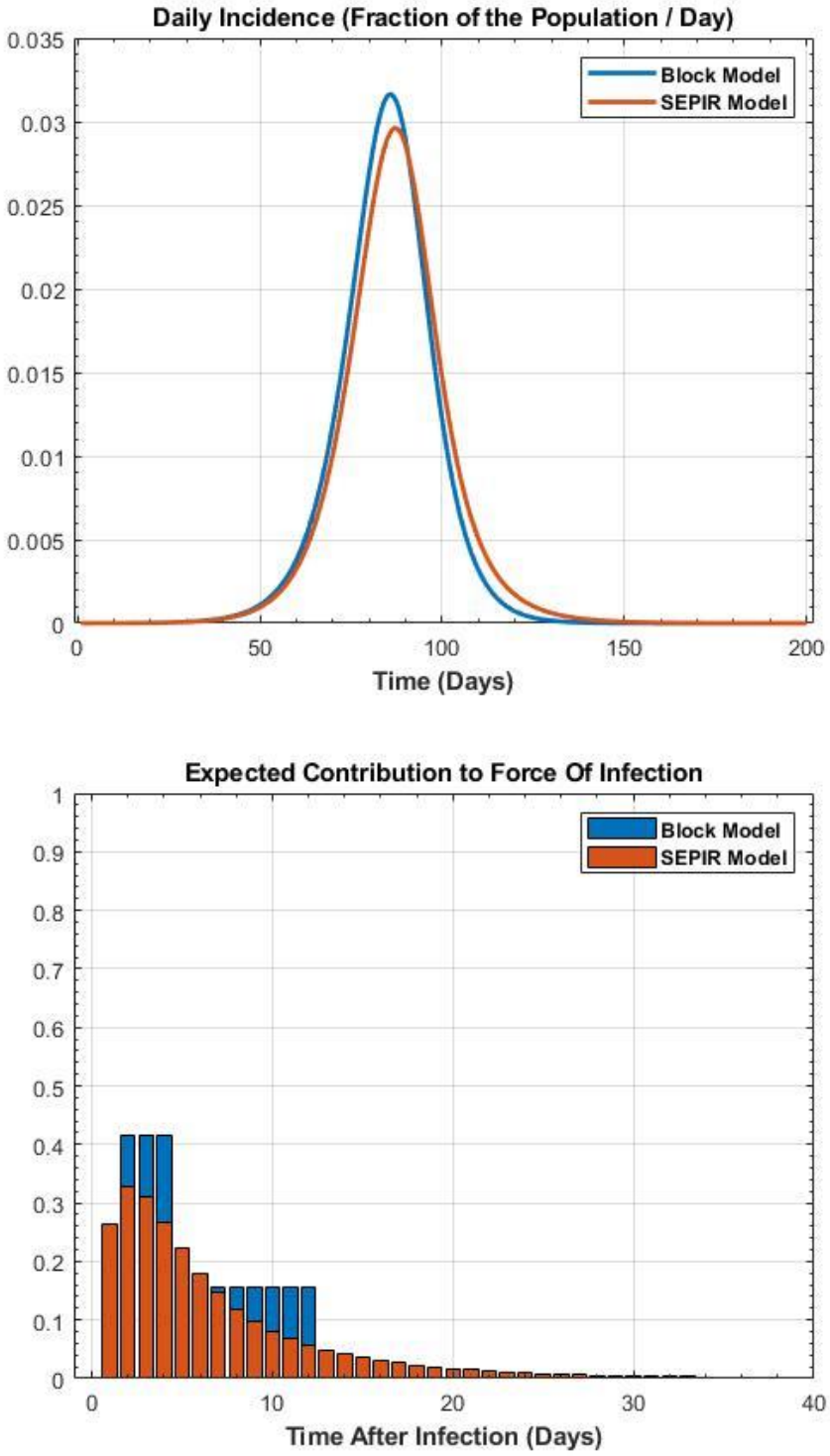

Figure 4.4: Top: Simulation of the daily incidence showing the 'Block Model' with deterministic periods (blue) and corresponding '$SEPIR$ Model' with stochastic periods (red) with the same R_0 and ρ. Corresponds to the parameters at which the ratio is minimal, $(T_E, T_P, T_I) = (2, 3, 8)$ and ρ = 1.1639. **Bottom:** The expected contribution to the force of infection for the 'Block Model' and '$SEPIR$ Model' at $(T_E, T_P, T_I) = (2, 3, 8)$.

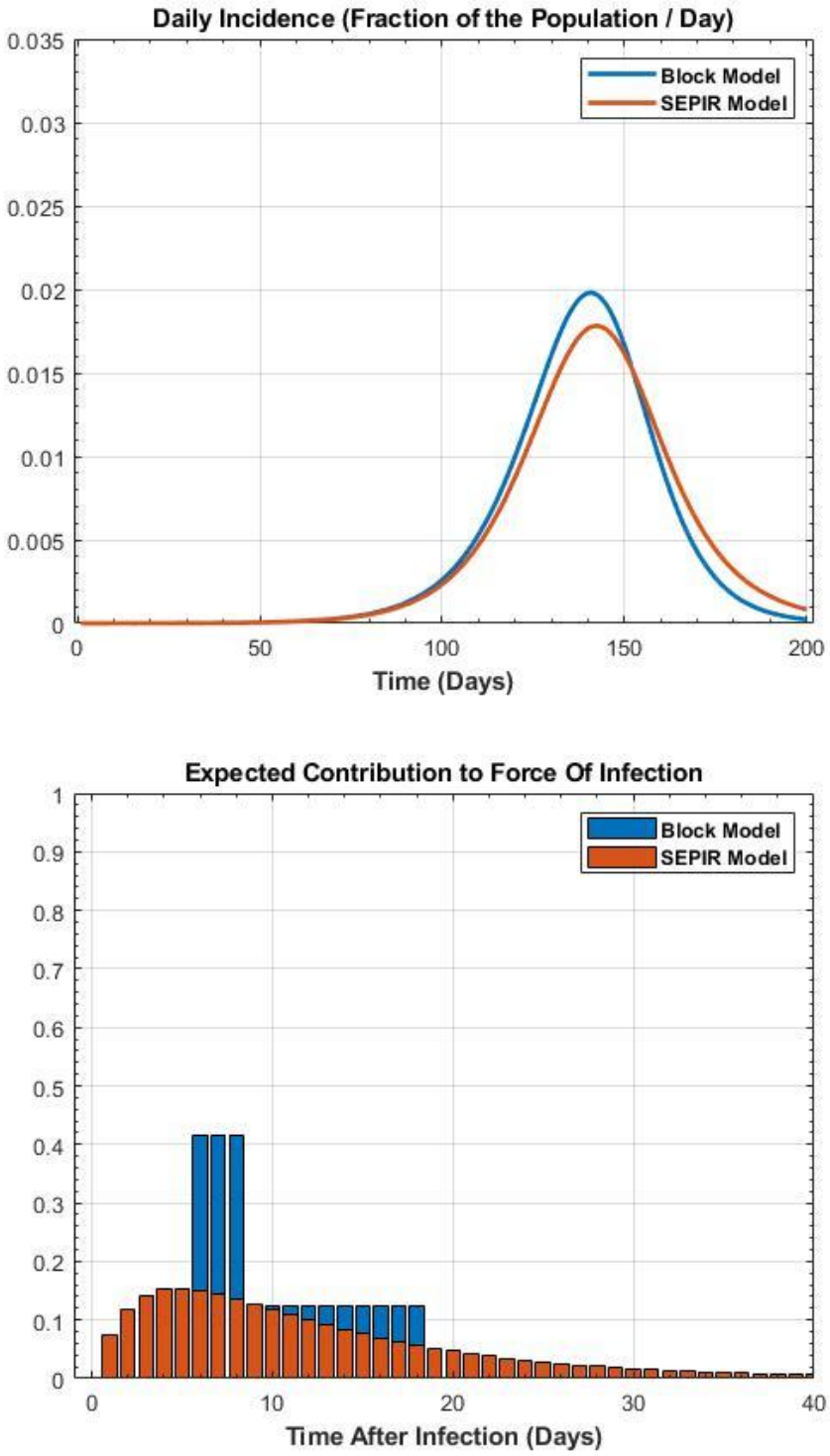

Figure 4.5: Top: Simulation of the daily incidence showing the 'Block Model' with deterministic periods (blue) and corresponding '$SEPIR$ Model' with stochastic periods (red) with the same R_0 and ρ. Corresponds to the parameters at which the ratio is maximal, $(T_E, T_P, T_I) = (6, 3, 10)$ and ρ = 1.0898. **Bottom:** The expected contribution to the force of infection for the 'Block Model' and '$SEPIR$ Model' at $(T_E, T_P, T_I) = (6, 3, 10)$.

The main results gathered from Figures 4.1, 4.2, and 4.3 are deterministic periods from the 'Block Model' lead to higher peaks than geometrically distributed periods from the compartmental '$SEPIR$ Model'. This is shown specifically when the exposed period is large, the pre-symptomatically infectious period is small, and the symptomatically infectious period is large. For reasonable parameter values, the difference is 7 – 11%.

From the parameters considered, at $(T_E,\ T_P,\ T_I) = (2,\ 3,\ 8)$, the relative difference in the peak incidences is minimal (Figure 4.4), while at $(T_E,\ T_P,\ T_I) = (6, 3, 10)$, the relative difference in the peak incidences is maximal (Figure 4.5).

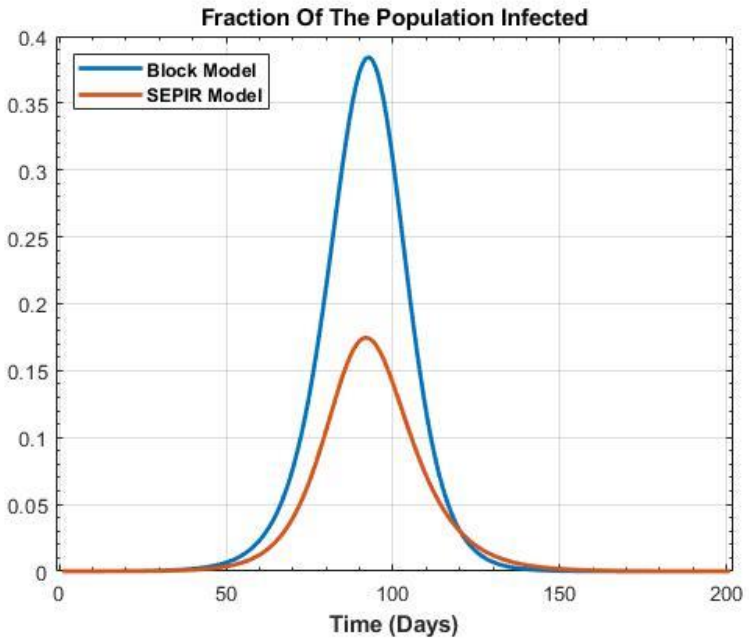

$(T_E, T_P, T_I) = (2,\ 3,\ 8)$

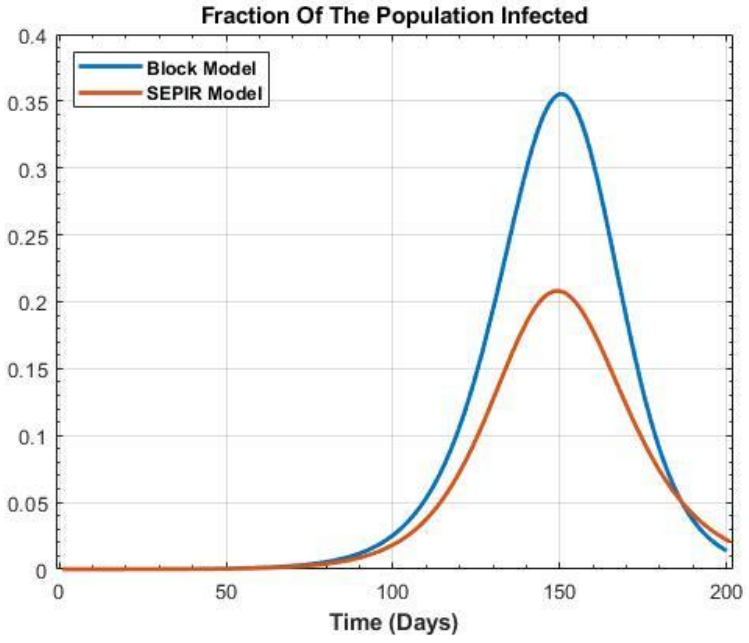

$(T_E, T_P, T_I) = (6,\ 3,\ 10)$

Figure 4.6: The fraction of the population that is either latently, pre-symptomatically infectious or symptomatically infectious in the 'Block Model' with deterministic periods (blue) and the corresponding '$SEPIR$ Model' with stochastic periods (red). **Top:** $(T_E,\ T_P,\ T_I) = (2,\ 3,\ 8)$ and **Bottom:** $(T_E,\ T_P,\ T_I) = (6, 3, 10)$. The corresponding incidences can be found in Figures 4.4 and 4.5, respectively.

Note that although the peak incidences in Figures 4.4 and 4.5 are not so very different, there is a large difference in the fraction of infected-and-not-yet-removed individuals in Figure 4.6, due to the comparatively fatter tail in the expected future contribution to the force of infection in the '$SEPIR$ Model'. Compartmental models have fatter tails, and they need, for given R_0, to have an earlier peak of infectiousness to have the same ρ. This can be seen in Figures 4.4 and 4.5 and eventually Figures 4.10 and 4.11.

An outbreak reaches its peak when S is reduced to the level corresponding to $R_0 = 1$. After the peak, the number of cases depends significantly on the number of individuals that are on the way to becoming or are infectious at the time the peak is reached. There is a fat tail in the time distribution for compartmental models until immunity is achieved. With the same R_0 and, therefore, final size, the supply of latent, pre-symptomatically and symptomatically infectious individuals is smaller at peak time than for models where the expected future infectiousness reduces to zero after a finite time. Reservoir size correlates with peak size, as shown in Figure 4.6. Lower peaks are expected, as the numerical results show.

4.3.2 'Actual Data', 'Weibull' Model (with Parameters corresponding to the Weibull Distribution) and '$SEPIR$ Model' with Stochastic Periods

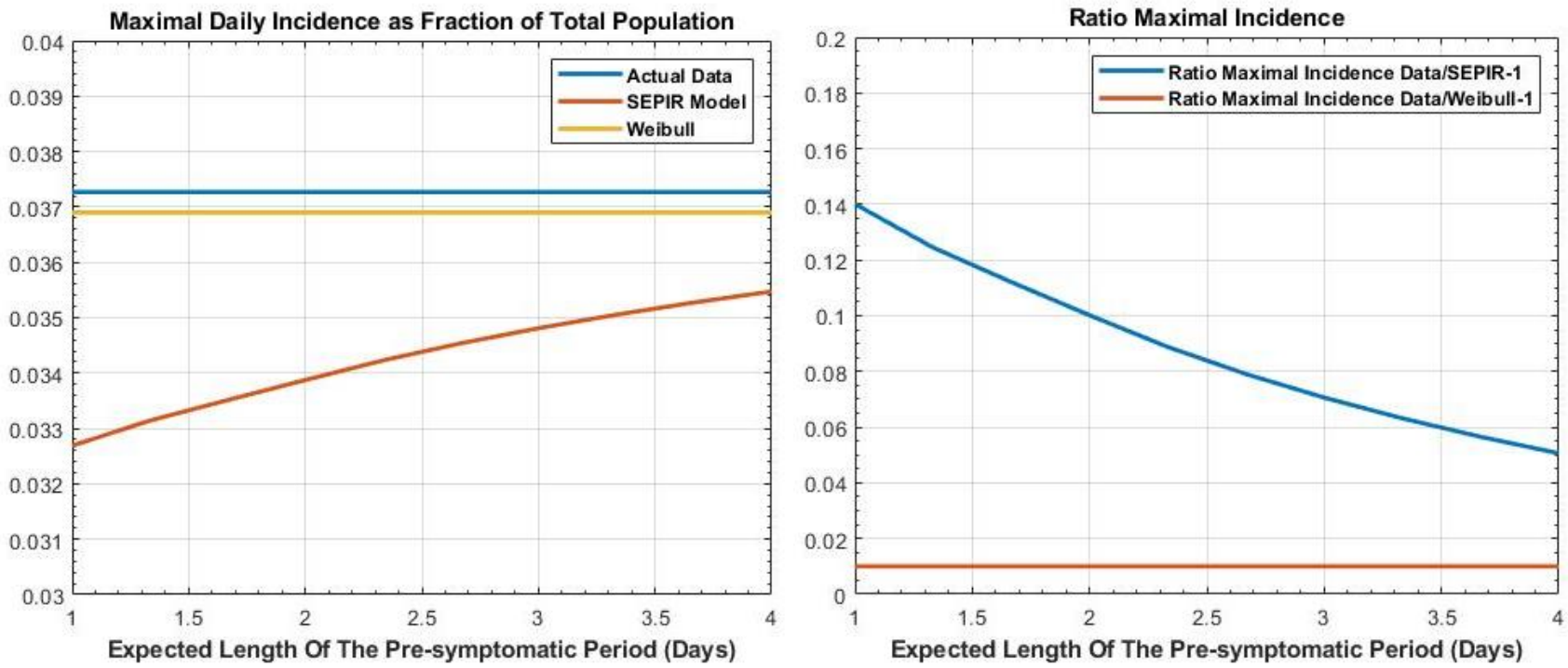

Figure 4.7: Left: 'Actual Data' (blue) obtained from generation-interval data [28] compared to the '$SEPIR$ Model' with stochastic periods (red) with the same R_0 and ρ. 'Weibull' Model (yellow) (with parameters formulated in [28] corresponding to the Weibull distribution) with the same reproduction number R_0 but a different growth rate ρ. **Right:** Relative ratio between the maximal incidences (-1, as in Figures 4.1, 4.2 and 4.3) as a function of T_P, the expected length of the pre-symptomatically infectious period when $T_E = 2$ and $T_I = 8$.

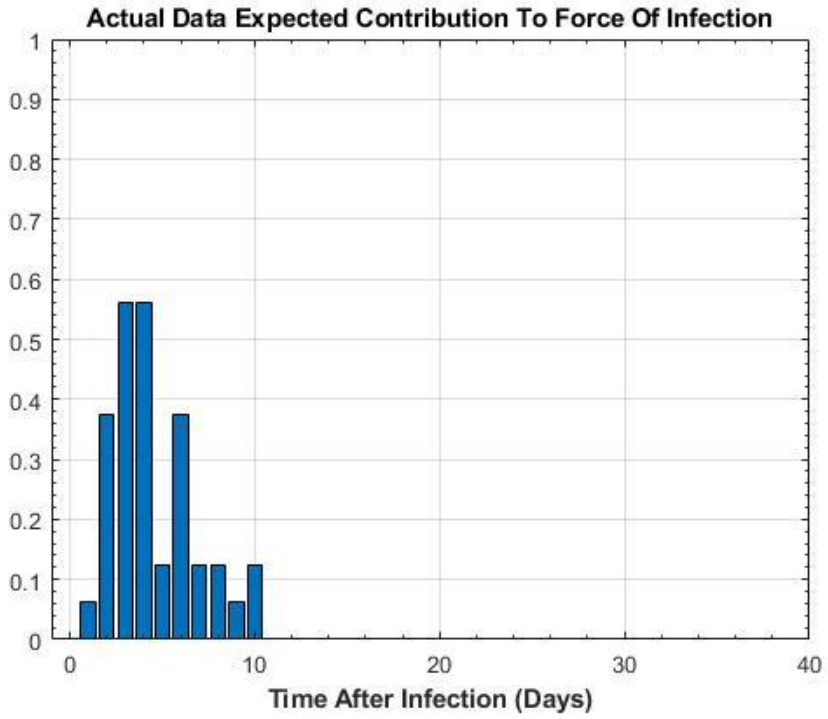

Figure 4.8: The expected contribution to the force of infection for the 'Actual Data.'

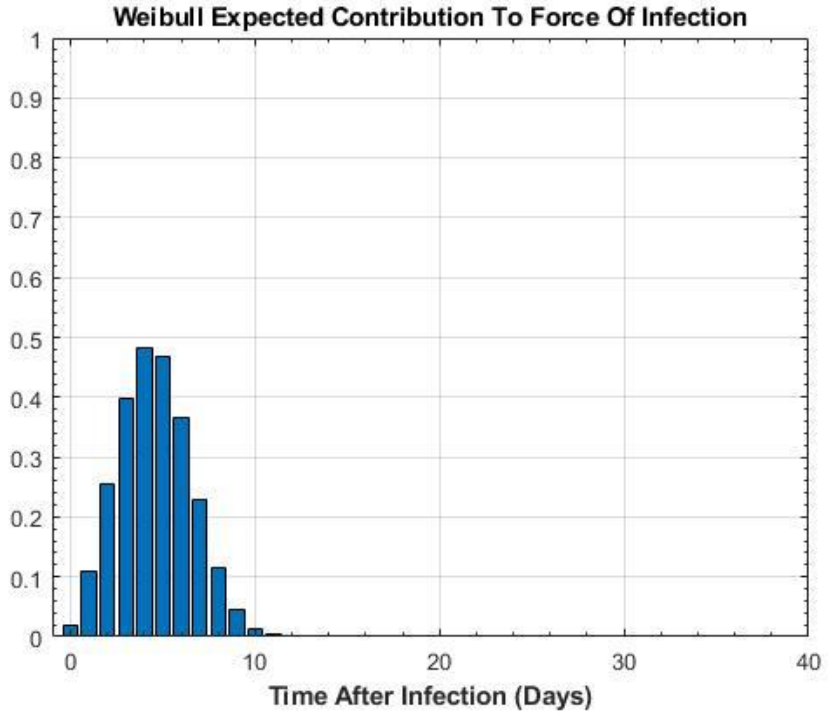

Figure 4.9: The expected contribution to the force of infection for the 'Weibull' Model.

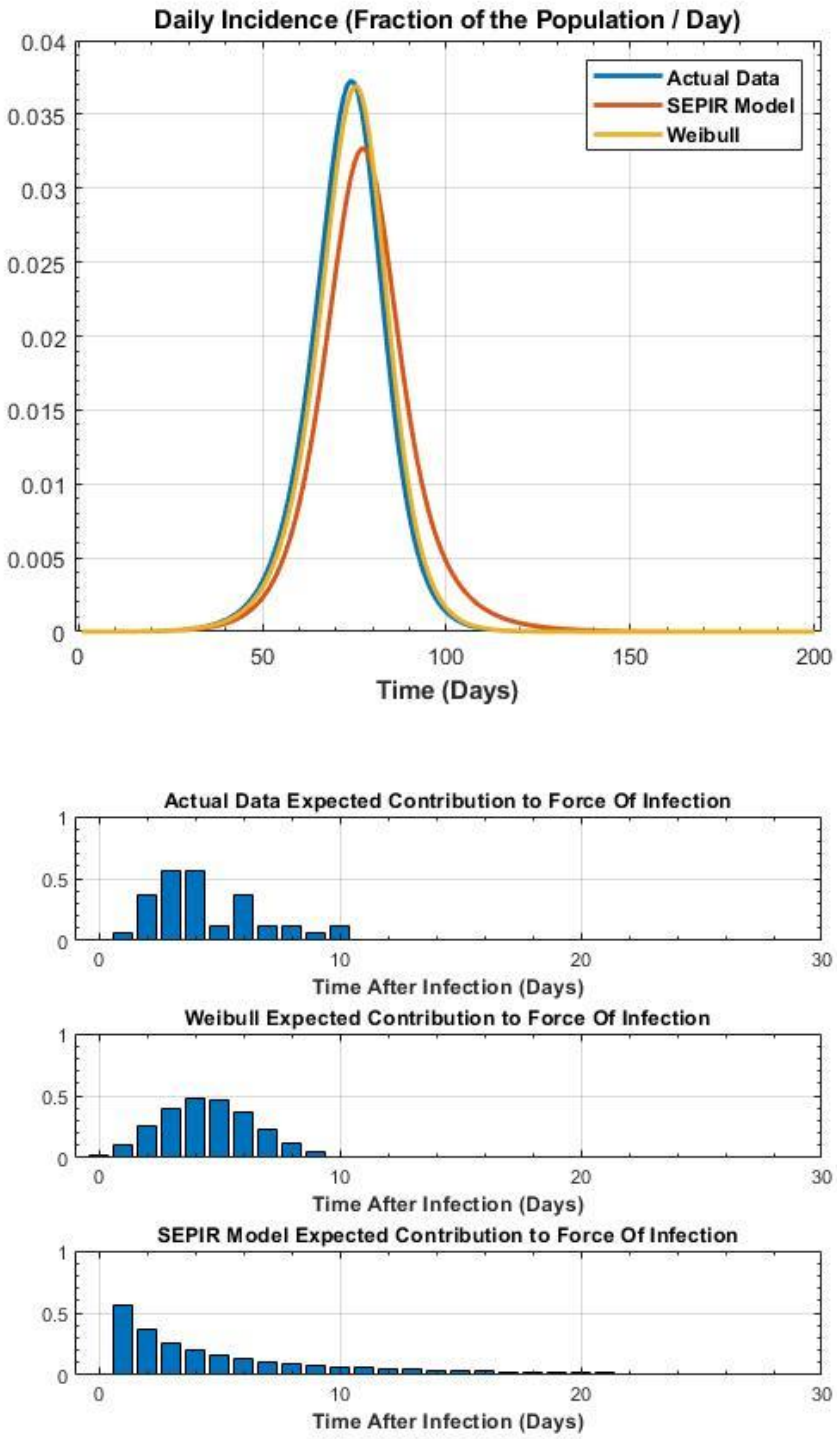

Figure 4.10: Top: Incidence of the 'Actual Data' (blue) [28] and the '$SEPIR$ Model' with stochastic periods (red) for $T_P = 1$ and ρ = 1.1961. The 'Weibull' Model (yellow) estimation from [28] was included with ρ = 1.1919. At this T_P, the relative difference in the peak incidences is maximal between the '$SEPIR$ Model' and 'Actual Data'. **Bottom:** The expected contribution of the 'Actual Data', 'Weibull' Model and '$SEPIR$ Model' for $T_P = 1$.

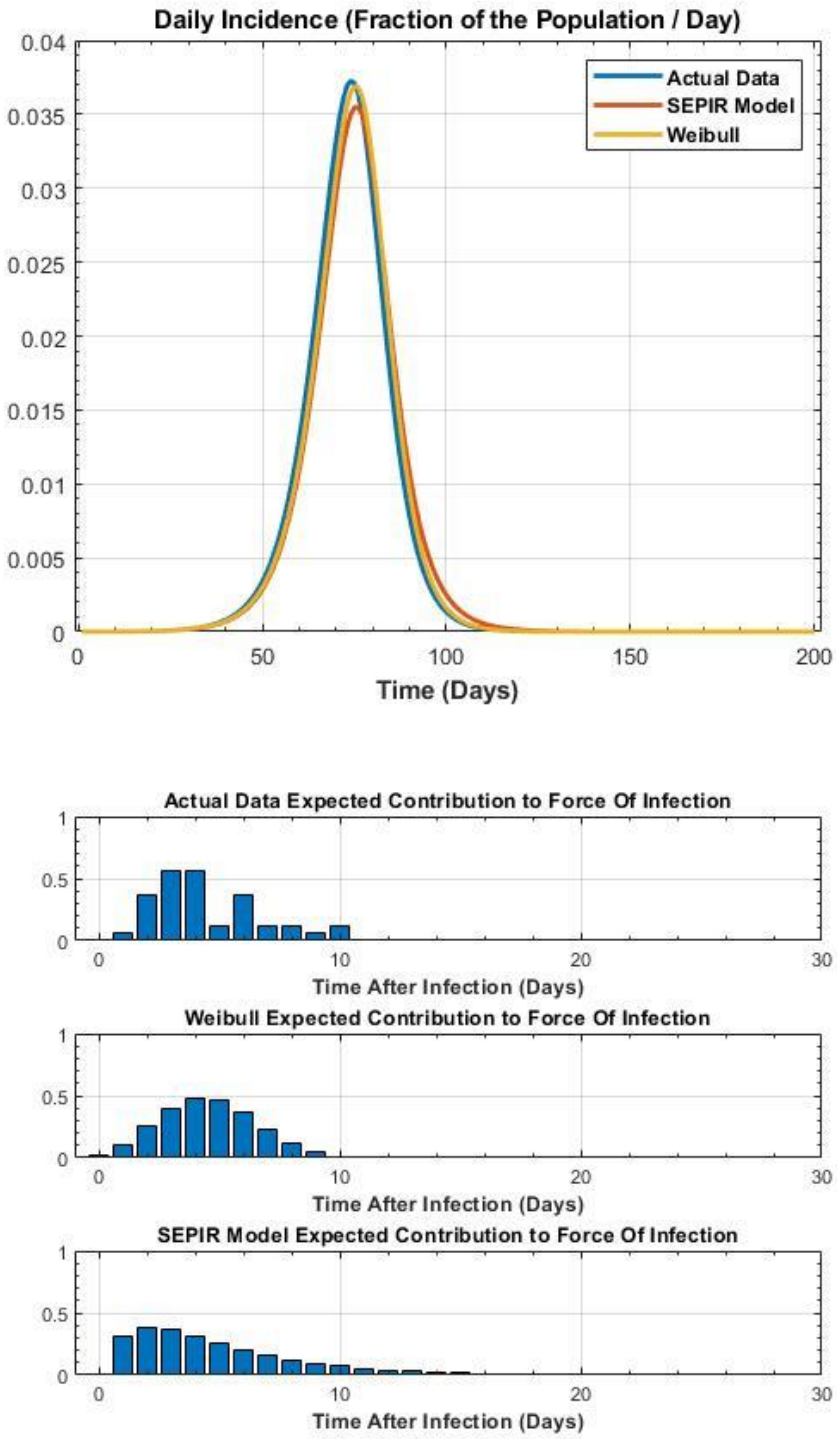

Figure 4.11: Top: Incidence of the 'Actual Data' (blue) [28] and the '$SEPIR$ Model' with stochastic periods (red) for $T_P = 4$ and ρ = 1.1961. The 'Weibull' Model (yellow) estimation from [28] was included with ρ = 1.1919. At this T_P, the relative difference in the peak incidences is minimal between the '$SEPIR$ Model' and the 'Actual Data'. **Bottom:** The expected contribution of the 'Actual Data', 'Weibull' Model and '$SEPIR$ Model' for $T_P = 4$.

The generation time distribution was directly estimated from 40 source-receipt pairs which is referred to as the 'Actual Data' here. These pairs were manually selected according to high confidence of direct transmission inferred from publicly available sources at the time of writing (March 2020) and with a known time of onset of symptoms for both source and recipient [28].

T_E and T_I are kept constant at 2 days and 8 days respectively with T_P varying between 1 and 4. From Figure 4.7 (Right), at $T_P = 1$, the relative difference in the peak incidences is maximal (Shown in details in Figure 4.10) and at $T_P = 4$, the relative difference in the peak incidences is minimal (Shown in details in Figure 4.11) between the '$SEPIR$ Model' with stochastic periods and the 'Actual Data'. For $T_P > 4.05$, the '$SEPIR$ Model' cannot be parameterized to have the same ρ as the 'Actual Data'.

The generation interval distribution was also approximated by a Weibull distribution derived from [28] with shape parameter 2.826 and scale parameter 5.665 but with a different ρ (1.1919). The peak differs by 1% from the 'Actual Data'. T_P does not affect the maximal daily incidence as a fraction of the total population for the 'Actual Data' and 'Weibull' Model as seen in Figure 4.7 (Left). The expected contribution to the force of infection for the 'Weibull' Model is only affected by changing the reproduction number, Weibull scale or shape parameter.

Just to clarify, the higher-peak-phenomenon matters in the COVID-19 context where on one hand, the parameters A_k as integrals over one-day time-intervals of the Weibull generation-time distribution as derived from the 'Actual Data' in [28] and on the other hand, determined by the one-parameter family of $SEPIR$ models that has R_0 equal to the 'Actual Data'. Only the '$SEPIR$ Model' has the same growth rate as the 'Actual Data'. The results of a comparison are presented in Figure 4.7 (Right), where the peak heights differ from 5 to 14% between the '$SEPIR$ Model' with stochastic periods and the 'Actual Data'.

Chapter 5

Discussion

This thesis aimed to establish the strength of a general discrete-time modelling framework in which model specification was reduced to the bare essentials. They are relatively simpler compared to continuous-time models, making them easier to execute and understand [4, 6, 7]. With the time steps being discrete in nature, it allows for straightforward computation and instinctive understanding of the model dynamics [4]. With calculations being performed at discrete time intervals, it can be computationally easier to simulate and analyze than continuous-time models [4]. With disease surveillance data collected and reported at discrete time intervals (daily, weekly, or monthly), discrete-time models line up well with this data availability [1, 4, 5]. This makes it easier to calibrate and validate the models with real-world observations [4]. They can be flexible for a variety of scenarios since they can include additional compartments and factors. They allow for the estimation of model parameters using statistical methods and are useful for evaluating the impact of interventions or control measures on disease spread [11]. The success of the $SEPIR$ Model variant towers over the attention of the general KM27 model. This is because the general model is developed as a renewal or Volterra integral equation. There are no user-friendly numerical tools available for computation to be done with such unfamiliar equations [4].

This thesis showed from the public health point of view, specific assumptions about the latent, pre-symptomatically infectious, and symptomatically infectious period matter for predicting the peak of the incidence curve. This can assist healthcare workers to be more prepared with enough PPE to perform their jobs without worrying about getting infected [16]. It can prevent overcrowding in the hospitals and help allocate medical resources such as more beds and respirators in the ICU

[23]. Government officials can be better able to enforce vaccination strategies and policies in certain demographics without facing public backlash [20]. Better preparation for future peaks and practicing COVID-19 protocols daily can help flatten the curve.

Two assumptions were made throughout this thesis. The first is the disease generates permanent immunity and the second is the host population is demographically closed. The results gathered from this are deterministic periods from the 'Block Model' led to higher peaks than geometrically distributed peaks from the '$SEPIR$ Model' implemented in this thesis which is similar to the results obtained in [4] for the $SEIR$ Model. This occurs when the latent period is large, the pre-symptomatically infectious period is small, and the symptomatically infectious period is large. For the parameter values considered, the difference is 7 – 11% whereas the $SEIR$ Model [4] and its 'Block Model' yielded a difference of 8 – 15% when T_E ranges from 3 to 6 days and T_I ranges from 4 to 9 days. The '$SEPIR$ Model' with stochastic periods has a limitation where A_k, the expected contribution to the force of infection is undefined when T_I equals T_P since it will result in a zero in the denominator.

Similarly, to the $SEIR$ Model in [4], in this thesis, the '$SEPIR$ Model' also showed that although the peak incidences are not so very different, there is a large difference in the fraction of infected-and-not-yet-removed individuals, due to the comparatively fatter tail in the expected future contribution to the force of infection.

Again the '$SEPIR$ Model' with stochastic periods developed in this thesis was compared to 'Actual Data' from [28] and a model given there with parameters corresponding to the Weibull distribution. The peak heights between the '$SEPIR$ Model' and the 'Actual Data' differ by 5 – 14% as T_P, the expected length of the pre-symptomatically infectious period changes from 1 to 4 days. As the number of days pre-symptomatically infectious increases, the difference in the peak height decreases so the peak of the '$SEPIR$ Model' approaches the peak of the 'Actual Data'. Whereas the $SEIR$ Model in [4] when compared to the Weibull distribution obtained a difference in peak height of 5 – 10% as its latent period changes from 1 to 4 days.

Heterogeneity has been ignored in this thesis but can be included to study the discrete-time model further while implementing additional compartments. While this thesis was largely focused on the

COVID-19 pandemic, the model can be adapted to other emerging infectious diseases with similar disease characteristics or vector-borne diseases, while updating disease-specific parameters.

Appendix A

Simulations with Different Initial Conditions

In this section, simulated results caused by changing initial conditions will be illustrated. Recall that for the results obtained in this thesis, $R_0 = 2.5$ was used to analyze the height and timing of the peaks. With the same total population ratio of 1, different reproduction numbers were introduced into simulations which were simulated for 400 days with an initial condition $s(t) = 1 - 0.000001\rho^{t+6}$, where $t = -1, -2, \ldots, -6$, as presented in Table A.1.

Figure A.1 shows the ratio maximal incidences between the 'Block Model' with deterministic periods and the '$SEPIR$ Model' with stochastic periods when $R_0 = 2$, $R_0 = 2.5$ and $R_0 = 3$ respectively. Their respective relative ratio of the peak heights is shown in Table A.2. When $T_I = 9$, the 'Block Model' has higher peaks than the '$SEPIR$ Model' as the reproduction number increases when $T_I = 9$. This is most prominent when the latent period is large, and the pre-symptomatically infectious period is small.

Parameter	Description		Value	Reference
R_0	Reproduction number		2 - 3	Assumed
ρ	Initial growth rate:	when $R_0 = 2$ when $R_0 = 2.5$ when $R_0 = 3$	1.0466 – 1.1149 1.0629 – 1.1600 1.0766 – 1.2003	Computed based on initial conditions
β_P	Pre-symptomatic transmission rate:	when $R_0 = 2$ when $R_0 = 2.5$ when $R_0 = 3$	0.1744 – 0.4398 0.1963 – 0.5248 0.2151 – 0.6074	Computed based on initial conditions
β_I	Symptomatic transmission rate:	when $R_0 = 2$ when $R_0 = 2.5$ when $R_0 = 3$	0.0545 – 0.0960 0.0810 – 0.1377 0.1088 – 0.1818	Computed based on initial conditions
$1/\gamma$	Mean latent period		2 – 7 days	Assumed
$1/\delta$	Mean infectious period of pre-symptomatic infection		3 – 8 days	Assumed
$1/\alpha$	Mean infectious period of symptomatic infection		9 days	Assumed

Table A.1: Description of the model parameters and their values when comparing the 'Block Model' with deterministic periods and the '$SEPIR$ Model' with stochastic periods for simulations with different reproduction numbers.

Ratio Maximal Incidence Block/SEPIR -1

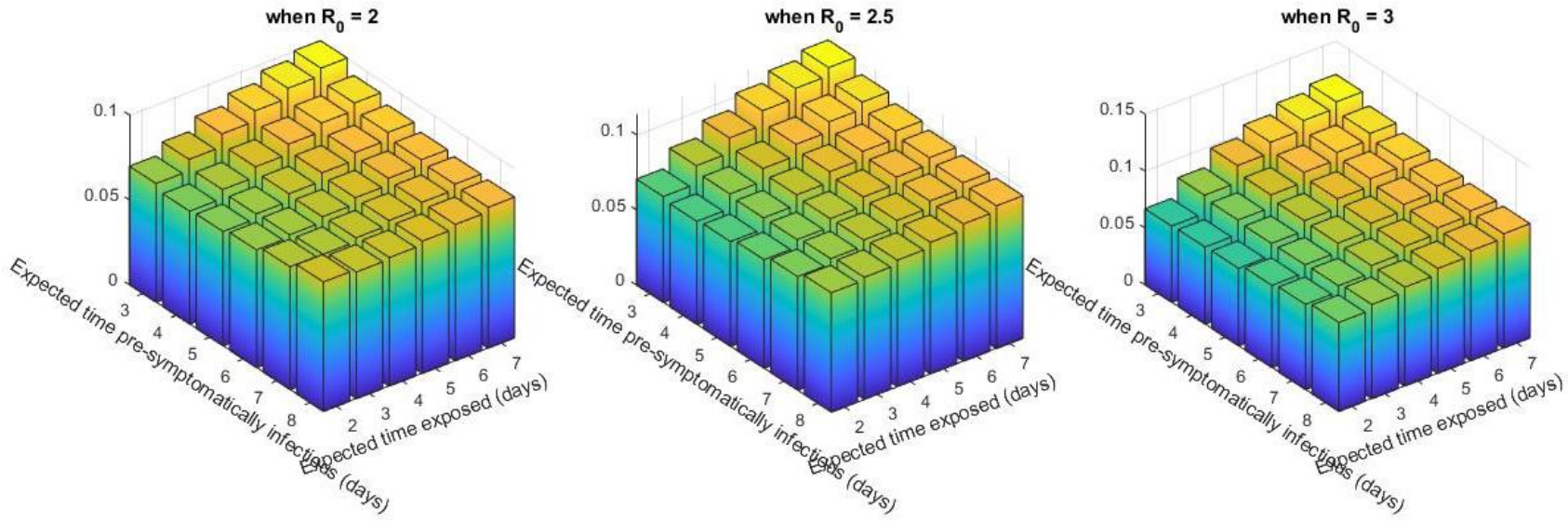

Figure A.1: The relative ratio between the 'Block Model' with deterministic periods and the '$SEPIR$ Model' with stochastic periods, as a function of T_E, the expected time individuals are exposed and T_P, the expected time individuals are pre-symptomatically infectious when **Left:** $R_0 = 2$, **Middle:** $R_0 = 2.5$ and **Right:** $R_0 = 3$.

$T_E \backslash T_P$	3	4	5	6	7	8
2	0.0699	0.0665	0.0674	0.0694	0.0723	0.0762
3	0.0767	0.0718	0.0703	0.0709	0.0722	0.0747
4	0.0843	0.0777	0.0747	0.0740	0.0745	0.0757
5	0.0904	0.0836	0.0796	0.0778	0.0772	0.0779
6	0.0962	0.0886	0.0840	0.0818	0.0805	0.0803
7	0.1006	0.0929	0.0884	0.0852	0.0837	0.0830

$T_E \backslash T_P$	3	4	5	6	7	8
2	0.0705	0.0686	0.0697	0.0723	0.0756	0.0794
3	0.0826	0.0784	0.0771	0.0772	0.0790	0.0812
4	0.0926	0.0869	0.0839	0.0827	0.0831	0.0842
5	0.1023	0.0945	0.0909	0.0887	0.0876	0.0876
6	0.1087	0.1010	0.0959	0.0934	0.0920	0.0914
7	0.1141	0.1057	0.1010	0.0978	0.0958	0.0950

$T_E \backslash T_P$	3	4	5	6	7	8
2	0.0670	0.0677	0.0682	0.0724	0.0748	0.0782
3	0.0829	0.0803	0.0789	0.0793	0.0801	0.0828
4	0.0978	0.0913	0.0878	0.0872	0.0867	0.0870
5	0.1071	0.0999	0.0958	0.0936	0.0923	0.0922
6	0.1150	0.1063	0.1024	0.0989	0.0974	0.0966
7	0.1204	0.1118	0.1073	0.1039	0.1014	0.1004

Table A.2: The relative ratio of the peak height of the two models ('Block Model' with deterministic periods and the '*SEPIR* Model' with stochastic periods) corresponding to Figure A.1 when **Top:** $R_0 = 2$, **Middle:** $R_0 = 2.5$ and **Bottom:** $R_0 = 3$.

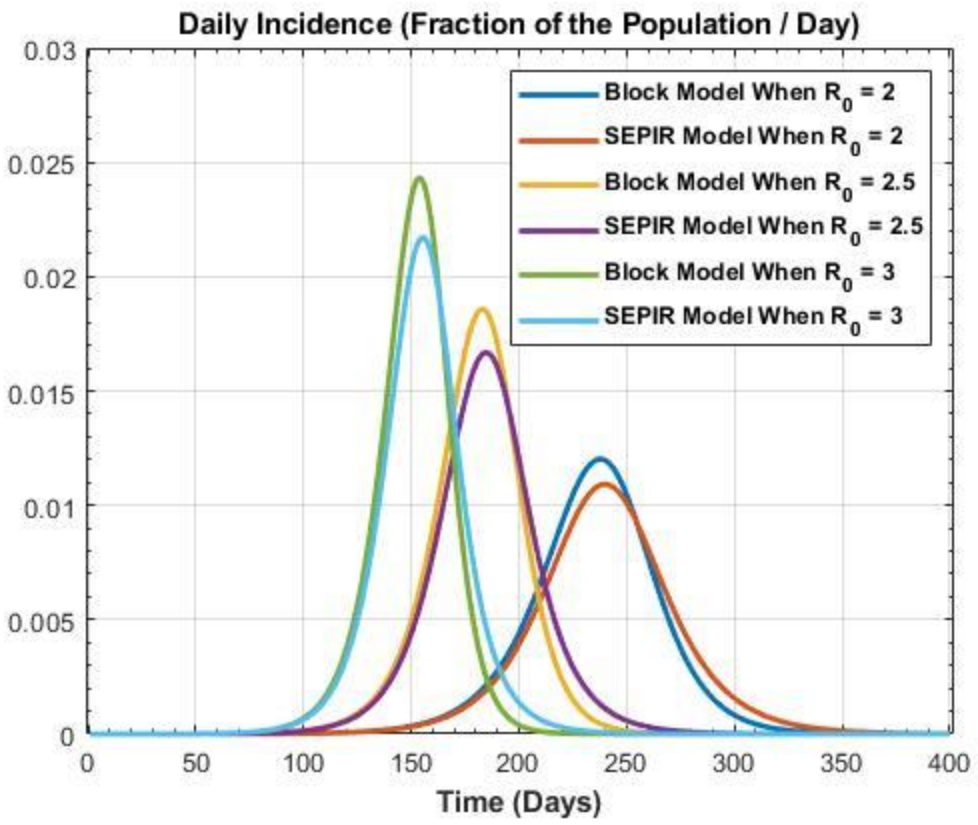

Figure A.2: Simulations of the daily incidence showing the 'Block Model' with deterministic periods and the '$SEPIR$ Model' with stochastic periods when $(T_E, T_P, T_I) = (7, 3, 9)$ for the different reproduction numbers.

Figure A.2 shows varying the reproduction number R_0 significantly changes the course of the epidemic over time. As R_0 increases, it causes the growth rate and the peak amplitude to increase, and peaks shift left therefore occurring at an earlier time in the epidemic. In Figure A.3, as R_0 increases for each model, the expected contribution to the force of infection increases for that specific day after infection.

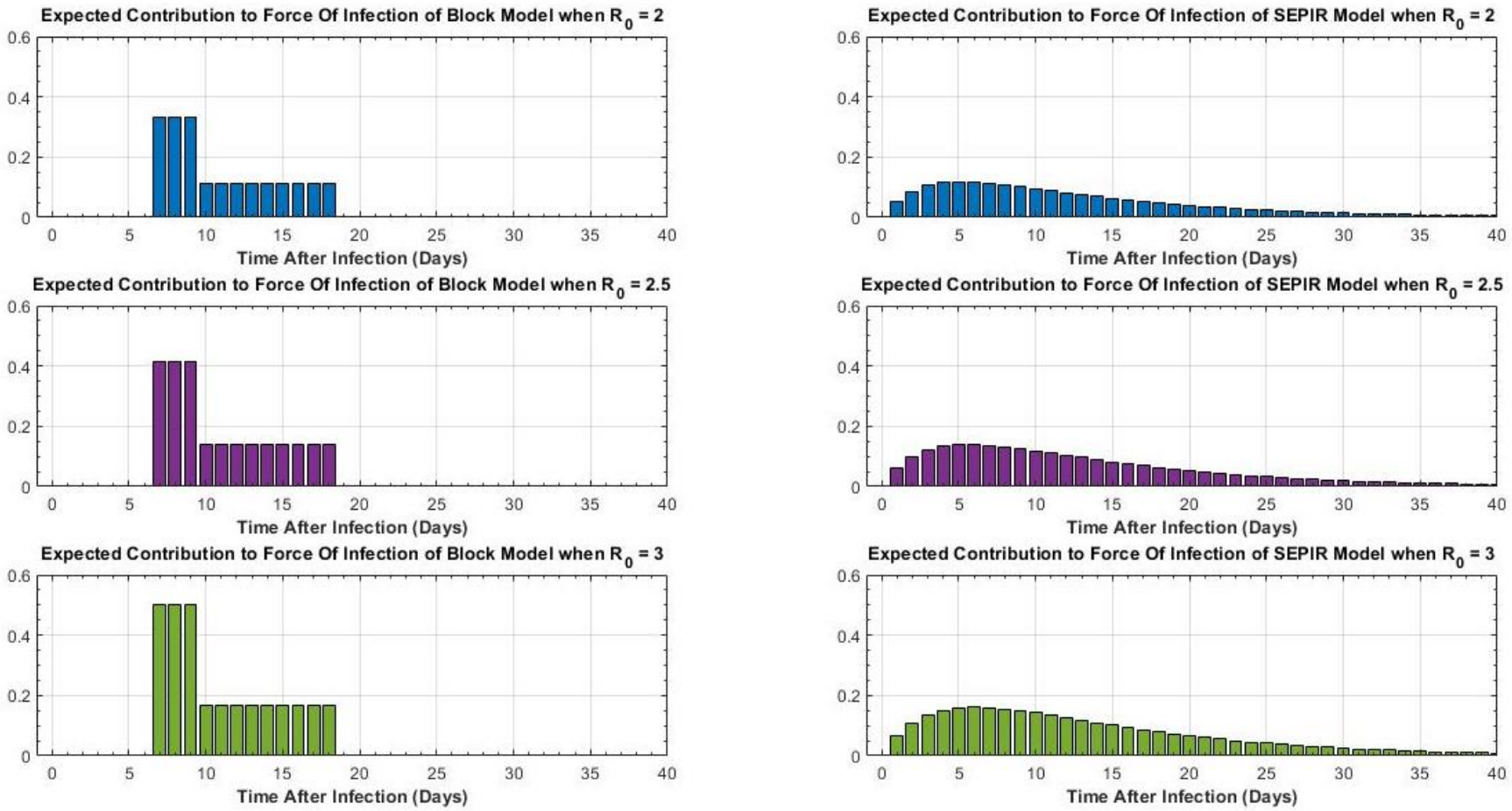

Figure A.3: The expected contribution to the force of infection for the 'Block Model' with deterministic periods and '$SEPIR$ Model' with stochastic periods at $(T_E,\ T_P,\ T_I)\ =\ (7,\ 3,\ 9)$ for the different reproduction numbers.

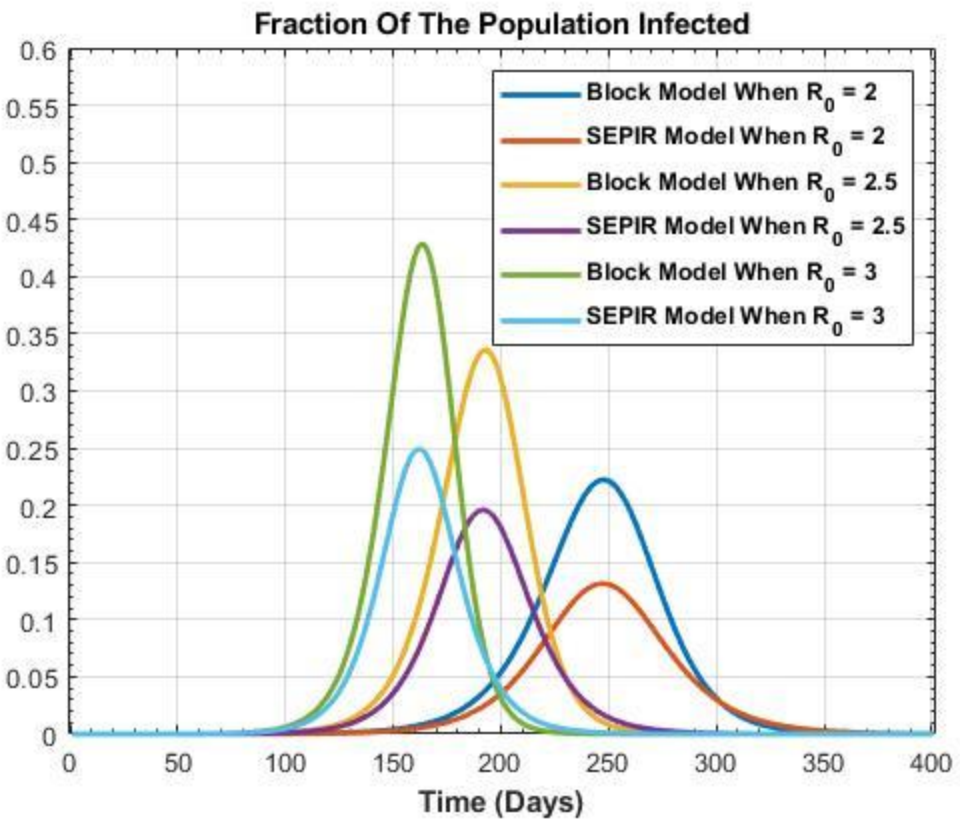

Figure A.4: The fraction of the population that is either latently, pre-symptomatically infectious or symptomatically infectious in the 'Block Model' with deterministic periods and the corresponding '$SEPIR$ Model' with stochastic periods for the different reproduction numbers when $(T_E, T_P, T_I) = (7, 3, 9)$. The corresponding incidences can be found in Figure A.2.

In Figure A.4, as R_0 increases, the peak fraction of the population infected shifts to the left (therefore occurring sooner) and the peak amplitude increases (since a greater fraction of the population would be infected). Also, the width of the peaks decreases, and this is due to the expected contribution to the force of infection and growth rate being greater, so infections occur at a faster rate. The '$SEPIR$ Model' has a fat tail in the expected contribution to the force of infection when compared to the 'Block Model' so the reservoir of latent and infectious individuals is smaller at peak time.

Bibliography

[1] Brauer, F., Feng, Z., & Castillo-Chavez, C. (2010). Discrete epidemic models. *Mathematical Biosciences and Engineering: MBE*, *7*(1), 1–15. https://doi.org/10.3934/mbe.2010.7.1.

[2] Bravo de la Parra, R., & Sanz-Lorenzo, L. (2021). Discrete epidemic models with two time scales. *Advances in Difference Equations*, *2021*(1), 478. https://doi.org/10.1186/s13662-021-03633-0.

[3] Brauer, F. (2009). Mathematical epidemiology is not an oxymoron. *BMC Public Health*, *9*(1), S2. https://doi.org/10.1186/1471-2458-9-S1-S2.

[4] Diekmann, O., Othmer, H. G., Planqué, R., & Bootsma, M. C. J. (2021). The discrete-time Kermack–McKendrick model: A versatile and computationally attractive framework for modeling epidemics. *Proceedings of the National Academy of Sciences*, *118*(39), e2106332118. https://doi.org/10.1073/pnas.2106332118.

[5] Getz, W. M., Salter, R., Muellerklein, O., Yoon, H. S., & Tallam, K. (2018). Modeling epidemics: A primer and Numerus Model Builder implementation. *Epidemics*, *25*, 9–19. https://doi.org/10.1016/j.epidem.2018.06.001.

[6] Ripoll, J., & Font, J. (2023). A Discrete Model for the Evolution of Infection Prior to Symptom Onset. *Mathematics*, *11*(5), 1092. https://doi.org/10.3390/math11051092.

[7] Breda, D., Diekmann, O., De Graaf, W. F., Pugliese, A., & Vermiglio, R. (2012). On the formulation of epidemic models (an appraisal of Kermack and McKendrick). *Journal of Biological Dynamics*, *6*(sup2), 103–117. https://doi.org/10.1080/17513758.2012.716454.

[8] Fares, A. (2011). Seasonality of Tuberculosis. *Journal of Global Infectious Diseases*, *3*(1), 46. https://doi.org/10.4103/0974-777X.77296.

[9] Getz, W. M., & Dougherty, E. R. (2018). Discrete stochastic analogs of Erlang epidemic models. *Journal of Biological Dynamics*, *12*(1), 16–38. https://doi.org/10.1080/17513758.2017.1401677.

[10] Yakubu, A.-A. (2021). A discrete-time infectious disease model for global pandemics. *Proceedings of the National Academy of Sciences*, *118*(42), e2116845118. https://doi.org/10.1073/pnas.2116845118.

[11] Yu, X., Liu, M., Zheng, Z., & Hu, D. (2023). Complex dynamics of a discrete-time SIR model with nonlinear incidence and recovery rates. *International Journal of Biomathematics*, *16*(08), 2250131. https://doi.org/10.1142/S1793524522501315.

[12] *Reduce respiratory Virus Spread Guide*. (2020, April 15). City of Toronto. https://www.toronto.ca/community-people/health-wellness-care/health-programs-advice/respiratory-viruses/covid-19/reduce-respiratory-virus-spread-guide/.

[13] Ranney, M. L., Griffeth, V., & Jha, A. K. (2020). Critical Supply Shortages—The Need for Ventilators and Personal Protective Equipment during the Covid-19 Pandemic. *New England Journal of Medicine*, *382*(18), e41. https://doi.org/10.1056/NEJMp2006141.

[14] Wynants, L., Calster, B. V., Collins, G. S., Riley, R. D., Heinze, G., Schuit, E., Albu, E., Arshi, B., Bellou, V., Bonten, M. M. J., Dahly, D. L., Damen, J. A., Debray, T. P. A., Jong, V. M. T. de, Vos, M. D., Dhiman, P., Ensor, J., Gao, S., Haller, M. C., … Smeden, M. van. (2020). Prediction models for diagnosis and prognosis of covid-19: systematic review and critical appraisal. *BMJ*, *369*, m1328. https://doi.org/10.1136/bmj.m1328.

[15] Telenti, A., Arvin, A., Corey, L., Corti, D., Diamond, M. S., García-Sastre, A., Garry, R. F., Holmes, E. C., Pang, P. S., & Virgin, H. W. (2021). After the pandemic: perspectives on the future trajectory of COVID-19. *Nature*, *596*(7873), 495–504. https://doi.org/10.1038/s41586-021-03792-w.

[16] *Shortage of personal protective equipment endangering health workers worldwide*. (2020, March 3). World Health Organization. https://www.who.int/news/item/03-03-2020-shortage-of-personal-protective-equipment-endangering-health-workers-worldwide.

[17] Cohen, J., & Rodgers, Y. van der M. (2020). Contributing factors to personal protective equipment shortages during the COVID-19 pandemic. *Preventive Medicine*, *141*, 106263. https://doi.org/10.1016/j.ypmed.2020.106263.

[18] Burki, T. (2020). Global shortage of personal protective equipment. *The Lancet. Infectious Diseases*, *20*(7), 785–786. https://doi.org/10.1016/S1473-3099(20)30501-6.

[19] Moghadas, S. M., Vilches, T. N., Zhang, K., Wells, C. R., Shoukat, A., Singer, B. H., Meyers, L. A., Neuzil, K. M., Langley, J. M., Fitzpatrick, M. C., & Galvani, A. P. (2021). The impact of vaccination on COVID-19 outbreaks in the United States. *medRxiv*. https://doi.org/10.1101/2020.11.27.20240051.

[20] *Ontario announces mandatory vaccine plans for health, education workers; 3rd doses for some*. (2021, August 18). CBC News. https://www.cbc.ca/news/canada/toronto/ontario-covid-vaccines-requirement-health-care-education-1.6143378.

[21] Wu, Z., & McGoogan, J. M. (2020). Characteristics of and Important Lessons From the Coronavirus Disease 2019 (COVID-19) Outbreak in China: Summary of a Report of 72 314 Cases from the Chinese Center for Disease Control and Prevention. *JAMA*, *323*(13), 1239–1242. https://doi.org/10.1001/jama.2020.2648.

[22] Grasselli, G., Pesenti, A., & Cecconi, M. (2020). Critical Care Utilization for the COVID-19 Outbreak in Lombardy, Italy: Early Experience and Forecast During an Emergency Response. *JAMA*, *323*(16), 1545–1546. https://doi.org/10.1001/jama.2020.4031.

[23] Ferstad, J. O., Gu, A., Lee, R. Y., Thapa, I., Shin, A. Y., Salomon, J. A., Glynn, P., Shah, N. H., Milstein, A., Schulman, K., & Scheinker, D. (2020). A model to forecast regional demand for COVID-19 related hospital beds. *medRxiv*. https://doi.org/10.1101/2020.03.26.20044842.

[24] Adalja, A. A., Toner, E., & Inglesby, T. V. (2020). Priorities for the US Health Community Responding to COVID-19. *JAMA*, *323*(14), 1343–1344. https://doi.org/10.1001/jama.2020.3413.

[25] Ferguson, N., Laydon, D., Nedjati Gilani, G., Imai, N., Ainslie, K., Baguelin, M., Bhatia, S., Boonyasiri, A., Cucunuba Perez, Z., Cuomo-Dannenburg, G., Dighe, A., Dorigatti, I., Fu, H., Gaythorpe, K., Green, W., Hamlet, A., Hinsley, W., Okell, L., Van Elsland, S., … Ghani, A. (2020). Report 9: Impact of non-pharmaceutical interventions (NPIs) to reduce COVID19 mortality and healthcare demand. *Imperial College London*. https://doi.org/10.25561/77482.

[26] Li, R., Pei, S., Chen, B., Song, Y., Zhang, T., Yang, W., & Shaman, J. (2020). Substantial undocumented infection facilitates the rapid dissemination of novel coronavirus (SARS-CoV-2). *Science*, *368*(6490), 489–493. https://doi.org/10.1126/science.abb3221.

[27] Murthy, S., Leligdowicz, A., & Adhikari, N. K. J. (2015). Intensive Care Unit Capacity in Low-Income Countries: A Systematic Review. *PLOS ONE*, *10*(1), e0116949. https://doi.org/10.1371/journal.pone.0116949.

[28] Ferretti, L., Wymant, C., Kendall, M., Zhao, L., Nurtay, A., Abeler-Dörner, L., Parker, M., Bonsall, D., & Fraser, C. (2020). Quantifying SARS-CoV-2 transmission suggests epidemic control with digital contact tracing. *Science*, *368*(6491), eabb6936. https://doi.org/10.1126/science.abb6936.

[29] Heesterbeek, J. A. P. (2002). A brief history of R0 and a Recipe for its Calculation. *Acta Biotheoretica*, *50*(3), 189–204. https://doi.org/10.1023/A:1016599411804.

[30] Heesterbeek, H. (2005). 5 – THE LAW OF MASS-ACTION IN EPIDEMIOLOGY: A HISTORICAL PERSPECTIVE. In K. Cuddington & B. E. Beisner (Eds.), *Ecological Paradigms Lost* (pp. 81–105). Academic Press. https://doi.org/10.1016/B978-012088459-9/50007-8.

[31] Pijpers, F. P. (2021). A non-parametric method for determining epidemiological reproduction numbers. *Journal of Mathematical Biology*, *82*(5), 37. https://doi.org/10.1007/s00285-021-01590-6.

[32] Park, S. W., Champredon, D., Weitz, J. S., & Dushoff, J. (2019). A practical generation-interval-based approach to inferring the strength of epidemics from their speed. *Epidemics*, *27*, 12–18. https://doi.org/10.1016/j.epidem.2018.12.002.

[33] Park, S. W., Sun, K., Champredon, D., Li, M., Bolker, B. M., Earn, D. J. D., Weitz, J. S., Grenfell, B. T., & Dushoff, J. (2021). Forward-looking serial intervals correctly link epidemic growth to reproduction numbers. *Proceedings of the National Academy of Sciences*, *118*(2), e2011548118. https://doi.org/10.1073/pnas.2011548118.

[34] Diekmann, O., Heesterbeek, H., & Britton, T. (2013). *Mathematical tools for understanding infectious diseases dynamics*. Princeton University Press.

[35] Moghadas, S. M., & Jaberi-Douraki, M. (2019). *Mathematical Modelling: A Graduate Textbook*. John Wiley & Sons.

[36] Bátkai, A., Kramar Fijavž, M., & Rhandi, A. (2017). *Positive Operator Semigroups* (Vol. 257). Springer International Publishing.

[37] Robinson, C. (1995). *Dynamical Systems: Stability, Symbolic Dynamics, and Chaos*. CRC Press.

[38] Kreck, M., & Scholz, E. (2020). Proposal of a recursive compartment model of epidemics and applications to the Covid-19 pandemic. *arXiv: Populations and Evolution*. https://doi.org/10.48550/arXiv.2009.00308.

[39] DeClerq, K. (2021, December 20). Ontario residents waiting days to get COVID-19 test, resulting in potential discrepancy in reported cases. *CTV News Toronto*. https://toronto.ctvnews.ca/ontario-residents-waiting-days-to-get-covid-19-test-resulting-in-potential-discrepancy-in-reported-cases-1.5714536.

[40] *Weibull Distribution*. (n.d.). MathWorks. https://www.mathworks.com/help/stats/weibull-distribution.html.

[41] Frost, J. (2023, May 4). *Weibull Distribution: Uses, Parameters & Examples.* Statistics By Jim. https://statisticsbyjim.com/probability/weibull-distribution/.

[42] *Why the Weibull Distribution is Always Welcome*. (2013, March 8). Minitab. https://blog.minitab.com/en/understanding-statistics/why-the-weibull-distribution-is-always-welcome.

[43] *Weibull Distribution*. (n.d.). ScienceDirect. https://www.sciencedirect.com/topics/physics-and-astronomy/weibull-distribution.

[44] *4.6: Weibull Distributions*. (2021, March 22). LibreTexts Statistics. https://stats.libretexts.org/Courses/Saint_Mary's_College_Notre_Dame/MATH_345__-_Probability_(Kuter)/4%3A_Continuous_Random_Variables/4.6%3A_Weibull_Distributions.

[45] Ma, Y., Wang, H., Huang, Y., Chen, C., Liang, S., Ma, M., He, X., Cai, K., Jiao, Z., Chen, L., Zhu, B., Li, K., Xie, C., Luo, L., & Zhang, Z. (2023). The Role of "Hierarchical and Classified Prevention and Control Measures (HCPC)" Strategy for SARS-CoV-2 Delta Variant in Guangzhou: A Modeling Study. *Journal of Epidemiology and Global Health*, *13*(2), 303–312. https://doi.org/10.1007/s44197-023-00108-1.